Quaternary Science Reviews 124 (2015) 48–67

Contents lists available at ScienceDirect

Quaternary Science Reviews

journal homepage: www.elsevier.com/locate/quascirev

Invited review

Interhemispheric dynamics of the African rainbelt during the late Quaternary

Joy S. Singarayer [a, *], Sallie L. Burrough [b]

[a] Department of Meteorology and Centre for Past Climate Change, University of Reading, RG6 6BB, UK
[b] Environmental Change Institute, University of Oxford, OX1 3QY, UK

ARTICLE INFO

Article history:
Received 20 October 2014
Received in revised form
15 June 2015
Accepted 19 June 2015
Available online xxx

Keywords:
Quaternary
Climate change
Africa
Intertropical Convergence Zone (ITCZ)
Tropical rainbelt

ABSTRACT

The spatial pattern of precipitation variability in tropical and subtropical Africa over the late Quaternary has long been debated. Prevailing hypotheses variously infer (1) insolation-controlled asymmetry of wet phases between hemispheres, (2) symmetric contraction and expansion of the tropical rainbelt, and (3) independent control on moisture available in Southern Africa via sea surface temperatures in the Indian Ocean. In this study we use climate-model simulations covering the last glacial cycle (120 kyr) with HadCM3 and the multi-model ensembles from PMIP3 (the Palaeoclimate Model Intercomparison Project) to investigate the long-term behaviour of the African rainbelt, and test these simulations against existing empirical palaeohydrological records. Through regional model-data comparisons we find evidence for the validity of several hypotheses, with various proposed processes occurring concurrently but with different regional emphasis (e.g. asymmetric shifts at the seasonal extremes and symmetric expansions/contractions towards West equatorial regions). Crucially, variations in rainfall are associated with multiple forcing mechanisms that vary in their dominance both spatially and temporally over the glacial cycle; an important consideration when interpreting and extrapolating from often relatively short palaeoenvironmental records.

1. Introduction

The climate of intertropical Africa is strongly governed by the dynamics of the tropical rainbelt, which is often associated with the Intertropical Convergence Zone (ITCZ) (Holton et al., 1971; Nicholson, 2009). Surface convergence has a strong influence on the tropical rainbelt in Africa but is not its sole driving mechanism and, as a consequence, the location of the ITCZ and the African rainbelt can markedly differ. Following Nicholson (2009), we deliberately distinguish the zone of maximum rainfall (the tropical rainbelt) from the ITCZ rather than use these terms interchangeably. Both the mean annual position and strength of the rainbelt are affected by the interhemispheric temperature gradient, which varies on seasonal to orbital scales. Over modern seasonal timescales, the oscillation of maximum insolation between hemispheres causes the rainbelt to track the summer temperature maximum, so that, away from the equator, the wet season is antiphased between northern (June, July, Aug) and southern (Dec, Jan, Feb) Africa (Fig. 1). Equatorial regions experience a bimodal pattern of rainfall seasonality (Fig. 1B) where the tropical rainbelt passes overhead twice a year as it moves north and then south. In many areas this double rainfall peak is unevenly distributed into 'long rains' and 'short rains', separated by a drier season.

Records of palaeoenvironmental change in North Africa clearly document the existence of 'wet phases' in the Sahara-Sahel and these appear to be paced by the 19–23 kyr periodicity of orbital precession, via its control on northern hemisphere summer insolation. Orbitally-induced peaks in summer insolation amplify the pressure difference between the continental landmass and the Atlantic Ocean, intensifying monsoonal circulation and potentially shifting the average position of the tropical rainbelt further north (DeMenocal et al., 2000; Braconnot et al., 2007; Patricola and Cook, 2007). The fluctuations between wet and dry phases in North Africa are recorded in a diverse range of palaeoproxies including vegetation composition, lake levels, dust emissions, and sapropel formation in the Mediterranean (e.g. DeMenocal et al., 2000; Demenocal et al., 1993; Lézine et al., 2011; Rossignol-Strick, 1983; Tjallingii et al., 2008). There is still vigorous debate on the role of biophysical feedbacks and the magnitude and abruptness of the resulting environmental changes (e.g. Brovkin and Claussen, 2008; Kröpelin

* Corresponding author.
E-mail address: j.s.singarayer@reading.ac.uk (J.S. Singarayer).

http://dx.doi.org/10.1016/j.quascirev.2015.06.021
0277-3791/

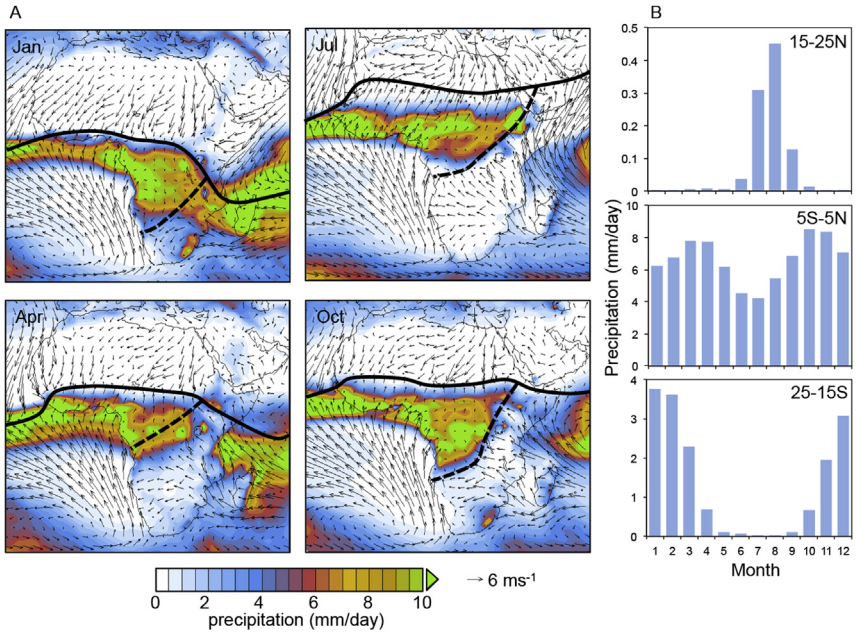

Fig. 1. A) Monthly mean precipitation in mm/day (filled contours) and 10 m winds from ERA Interim renanalysis (1979–2013 average; Dee et al., 2011). Black lines illustrate the main zone of intertropical convergence. Dashed black lines illustrate the Congo Air Boundary. B) Seasonality of precipitation over a central latitudinal cross-section of Africa (15–30°W).

et al., 2008; Claussen et al., 2013), but there is a strong consensus (e.g. Huang et al., 2008) that the periodic 'greening' of the Sahara, the most recent being the African Humid Period (14.5–5.5 kyr), is causally related to orbitally driven increases in northern hemisphere summer insolation (Pokras and Mix, 1987; Prell and Kutzbach, 1987).

In sub-Saharan Africa and in southern Africa in particular, the pacing and nature of long-term environmental change is less clear (Burrough and Thomas, 2013; Govin et al., 2014) and there is little consensus on the role of direct insolation forcing as a causal mechanism for observed changes in palaeo-rainfall records and the behaviour of the African rainbelt during the Quaternary. This lack of coherence is due in part to the fragmentary nature of available empirical data and the paucity of long, continuous, high-resolution records of palaeoenvironmental change in the southern hemisphere tropics. In addition, the land mass/ocean configuration of Africa south of the equator may add spatial complexity to the climate system response to forcing (Lee Thorp et al., 2004; Burrough and Thomas, 2013) in comparison to the more homogeneous response of northern Africa.

Direct insolation control of hydroclimate (and by extension, the predicted pattern of anti-phased responses between hemispheres – further discussion below) is best detectable in climate signals when the amplitude of the precessional cycle, modified by eccentricity, is at its greatest. It is possible therefore to predict periods of time during the Quaternary, such as the last interglacial, when hydroclimatic changes might be more visible in long palaeoclimate records (supplementary information, Fig. S1). However, one of the difficulties of assessing the relative importance of insolation control on African climate stems from the scarcity of continuous high-resolution palaeoclimate records that extend beyond the Holocene (when the amplitude of insolation forcing is relatively small). Longer time series that capture the last Interglacial (~130–115 kyr) do indeed suggest that this was a period when palaeoclimate underwent high amplitude changes linked to precession (Burnett et al., 2011; Cohen et al., 2007; Moernaut et al., 2010; Scholz et al., 2007; Trauth et al., 2003). When the amplitude of precessional variability is low, direct insolation control as a driver of climate may be muted and other forcing mechanisms, including high latitude events and long-term greenhouse-gas (GHG) variation, may become relatively more important for determining climate responses (Kuechler et al., 2013; Tjallingii et al., 2008).

Several alternative hypotheses concerning the main drivers of intertropical rainfall change in the late Quaternary have emerged in recent years in response to new palaeorecords that do not fit the idea of hemispheric asymmetry driven by local insolation variations. These include the periodic expansion and contraction of the rainbelt causing a symmetrical pattern of palaeorainfall trends between the northern and southern hemispheres; the zonal movement of the rainbelt, particularly associated with the Congo Air Boundary (CAB) and the role of sea surface temperatures (SST) in the Indian Ocean as a driver of terrestrial rainfall. There is intense debate about the validity of these seemingly conflicting models of palaeohydroclimate change, which is difficult to resolve with the spatiotemporal resolution of the existing palaeoenvironmental archive. As such, climate model simulations may provide useful insights into the primary controls on late Quaternary tropical rainfall variations. The aim of this study is to: i) review the current theoretical models (section 2); ii) use HadCM3 climate model simulations covering the late Quaternary as well as multi-model ensemble simulations (methods described in section 3), in conjunction with long palaeohydrological records, to examine the applicability of the above hypotheses in different regions (section 4); iii) reflect on the proposed mechanisms, and suggest where future data collection and synthesis would be most useful to differentiate between conflicting findings or to better resolve the spatial extent of regional patterns of change (section 5).

2. Theoretical models

Here, we outline the prevailing ideas commonly employed to explain palaeo-rainfall data across Africa. The records we use to illustrate these models are selected for their length, continuity, and

relevance to the hypotheses discussed below (Fig. 2, Table 1). We have not included qualitative data (e.g. where pollen composition is used to infer a change in rainfall without a quantitative interpretation) or palaeoenvironmental records shorter than 10 kyrs. We have also tried to avoid using discontinuous data except where it serves to test specific model outcomes. This is not a judgement on the quality of these data but instead is driven by the need for palaeodata that is directly comparable with model data outputs.

2.1. Interhemispheric asymmetry

The effect of orbital precession is to cyclically modify the *seasonal* distribution of insolation between hemispheres with approximately 23-kyr periodicity such that 10 kyrs ago, summer insolation in the north African subtropics was ~8% more intense than today (warmer summers, colder winters) while in the southern sub-tropics the opposite was true (Berger, 1978). Because the intensity of low-latitude rainfall is controlled by summer season insolation, the logical extension of this theory, supported by several climate-model simulations (Kutzbach et al., 2008; Liu et al., 2003) is that 'wet periods' will be anti-phased between hemispheres on the African continent over orbital timescales. In a seminal paper by Partridge et al. (1997b) documenting a 200-kyr rainfall record derived from the Tswaing Crater in southern Africa, a strong correlation was found between enhanced North African monsoons and reduced rainfall in southern Africa. These data provided the first strong empirical evidence to support the notion that both subtropical northern *and* southern African climate were responsive to precessionally driven changes in summer-season insolation and that these responses were out-of-phase between hemispheres (Fig. 3a). Despite strong criticisms over the last decade for its poorly constrained and tuned age model, the Tswaing crater proxy rainfall data (Fig. 3a) has remained the only continuous, terrestrial hydroclimate record in South Africa to extend beyond the last glacial.

New archives of palaeoenvironmental change from central, eastern, and southern Africa, many of which do not conform to a simple model of hemispheric asymmetry, have led researchers to question or modify the mechanism of direct insolation control on African climate. In Eastern Africa, an emerging network of palaeoproxy data suggests that the climatic 'hinge zone', which separates sites with an apparent 'northern mode' of orbital scale climate variability from those sites with a 'southern mode' responding directly to southern hemisphere insolation forcing (Barker and Gasse, 2003, Tierney et al., 2011a; Shefuß et al., 2011; Costa et al., 2014), lies south of the equator. Geographically, this divide appears to occur just north or west of Lakes Malawi/Masoko which generally exhibit a southern mode of hydroclimate variability (Konecky et al., 2011; Garcin et al., 2006) (Fig. 4). To the south, a ~17-kyr leaf-wax δD record from the Zambezi basin (site 14) and a 140-kyr southeast Atlantic leaf-wax δD record derived from the Kalahari desert (site 9) (Fig. 6) are more consistent with the notion that hydroclimate variability has been strongly influenced by direct southern hemisphere insolation control (Collins et al., 2014; Schefuß et al., 2011). Other southerly sites, such as the Makgadikgadi basin (Fig. 6), may add complexity to this pattern through their size and catchment geography, and the fact that the lacustrine basin itself lies south of the 'hinge zone' but is fed by moisture in the central African tropics, strongly influenced by a northern mode of hydroclimate variability that controls the west African monsoon (Burrough and Thomas, 2013; Burrough et al., 2009a).

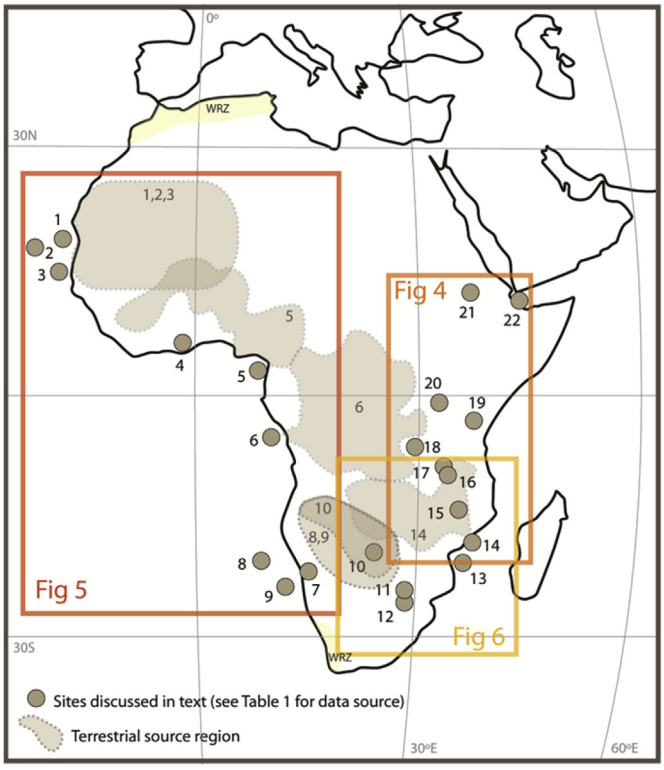

Fig. 2. Principal sites discussed in text. Terrestrial source regions for some oceanic cores are shown in grey and labelled with the relevant site number. Site details are provided in Table 1 below and palaeoproxy time-series are shown in Figs. 4–6. Winter rainfall zones (i.e. not dominantly impacted by the behaviour of the intertropical rainbelt are shown in yellow and not considered further in this paper). (For interpretation of the references to colour in this figure legend, the reader is referred to the web version of this article.)

2.2. Symmetry across the equator: expansion and contraction of the African rainbelt

Terrestrially derived organic and sedimentary markers from marine sediment cores spanning the western margin of tropical Africa suggest that, rather than an asymmetric pattern of hydroclimate change between the northern and southern modes, the African rainbelt contracted and expanded symmetrically in both hemispheres (Collins et al., 2011). In this model, the dominant dynamic of the African rainbelt is in terms of the latitudinal range of seasonal movement, increasing or decreasing the average length of the rainy season (Collins et al., 2011). The idea that southwest African hydroclimate effectively responds in phase with northern hemisphere Africa is supported by other proxies from southwest Africa including stable nitrogen-isotope records from hyrax middens interpreted as an indicator of moisture availability (Chase et al., 2010, 2009) (Fig. 5A) leading researchers to suggest that Southern Africa underwent a 'progressive aridification' during the Holocene synchronously with declining humidity characterising the North African Humid Period.

2.3. Diverging patterns of hydroclimate across an east-west gradient and the role of the Congo Air Boundary (CAB)

High lakes and apparent wetter conditions are similarly found to occur periodically in equatorial East Africa in phase with the North African humid periods (e.g. Gasse et al., 2008; Costa et al., 2014; Tierney and deMenocal, 2013; Garcin et al., 2009; Berke et al., 2012). Changes in insolation and shifts in the mean annual position of the ITCZ do not adequately explain this long term hydroclimate variability, particularly as this behaviour extends south of the equator to southeast African lakes, including Rukwa

Table 1
Principal site locations and details of empirical data discussed in text.

Site no.	Site description	Latitude	Longitude	Proxy	Time range of record (ka)	Reference
1	Offshore Mauritania (GeoB7920-2)	20.75	−18.58	Continental humidity index (grain-size analyses)	116–0.5	Tjallingii et al., 2008
2	Cape Verde Plateau (ODP Site 659)	18.08	−21.03	C_{31} δDwax	131–2.5	Küchler et al., 2013
3	Offshore Senegal (GeoB9508-5)	15.50	−17.95	C_{31} δDwax	43.6–1.4	Niedermeyer et al., 2010
4	Lake Bosumtwi	6.51	−1.41	% LOI organic content	26.7–0.2	Peck et al., 2004
5	Gulf of Guinea (MD03-2707)	2.5	9.4	Ba/Ca (riverine runoff/SSS)	156–0.4	Weldeab et al., 2007
6	Congo River Mouth	−5.94	11.47	C_{29} δDwax	19.5–0.03	Schefuβ et al., 2005
7	Spitzkoppe	−21.82	15.18	Hydrax midden $\delta^{15}N$	11.8–0.05	Chase et al., 2009
8	Walvis Ridge (MD962094)	−20	9.27	Continental aridity index (grain-size analyses)	321–4	Stuut et al., 2004
9	Offshore Nambia (MD08-3167)	−23.32	12.38	C_{31} δD δDwax	136–1.5	Collins et al., 2014
10	Makgadikgadi basin sump	−20.62	25.36	Shoreline OSL	288–8.4 (discontinuous)	Burrough et al., 2009a
11	Wonderkrater	−24.43	28.75	Pollen derived wet season rainfall	19.7–0.3	Truc et al., 2013
12	Tswaing Crater	−25.56	28.75	Grain size	199–0.02	Partridge et al., 1997a, 1997b
13	Indian Ocean (MD79257)	−20.4	36.33	Sea surface temperature from Uk'37	45–1.2	Bard et al., 1997
14	GeoB9307-3 Zambezi Delta	−18.56	37.38	C_{28} δDwax	16.9–0.3	Schefuβ et al., 2011
15	Lake Chilwa	−15.5	35.3	Shoreline OSL	44–0 (discontinuous)	Thomas et al., 2009
16	Lake Malawi	−10	34	C_{28} δDwax	78.9–0.1	Konecky et al.;, 2011
17	Lake Masoko	−9.33	33.75	Low-field magnetic susceptibility	45.3–0.03	Garcin et al., 2006
18	Lake Tanganyika	−6.71	29.83	C_{28} δDwax	59.5–1.4	Tierney et al., 2008, 2010
19	Lake Challa	−3.3	37.7	BIT index	25–0.05	Verschuren et al., 2009
20	Lake Victoria	−1.23	33.20	C_{28} δDwax	14.9–1.4	Berke et al., 2012
21	Lake Tana	12	37.35	C_{28} δDwax	15.1–1.4	Costa et al., 2014
22	Gulf of Aden	12	44.3	C_{30} δDwax	40.1–0	Tierney and deMenocal 2013

(Vincens et al., 2005), Cheshi (Stager, 1988) and Tanganyika (Burnett et al., 2011; Tierney et al., 2008). Using simulations with the GISS Model E-R of the mid-Holocene (6 kyr BP), Tierney et al. (2011a) have argued that an increase in available moisture can be attributed to a reduction in southern equatorial East African seasonality (i.e. a wetter dry season (June–Nov) and drier wet season (Dec–May)) (Tierney et al., 2011a). The theory asserts that increased P-E (precipitation minus evaporation) during the dry season had a major impact on the cumulative annual water balance and vegetation response but the decreased wet season P-E had less hydrological impact so that the overall response was mean higher lake levels in spite of little change in mean annual P-E. Mechanistically, it argued this East African hydroclimatic shift was an indirect response to insolation caused by a change in the zonal advection of moisture from both the Atlantic and Indian Ocean. To the west, enhanced low pressure over North Africa during the summer wet season and the development of a dipole SST anomaly in the tropical Atlantic caused the trade winds to weaken and allowed an increase of westerly moisture flux inland from the Atlantic (Kutzbach and Liu, 1997; Tierney et al., 2011a). At the same time, heating of the southern half of the continent set up a pressure differential with the SE Atlantic, which remained cool following reduced winter insolation in the southern Hemisphere. This pressure gradient also pulled in moisture from the Atlantic. Therefore in the mid-Holocene during Sept-Oct-Nov within the equatorial region, and slightly south of it, an intensification of precipitation occurred in the regions affected by convergence along the Congo Air Boundary (CAB). In addition, warmer SSTs in the Indian Ocean related to the Indian Monsoon, resulted in increased moisture advection on to easternmost Africa.

The Congo Air Boundary (CAB; Fig. 1) is a zonal extension of the ITCZ which marks the confluence between Atlantic and Indian Ocean derived moisture. Variations in the Atlantic moisture flux, which converges and precipitates at the CAB, are now commonly cited as a key driver of the observed spatial and temporal pattern of hydroclimate change across Africa (Costa et al., 2014; Tierney et al., 2011b). In particular, the long term behaviour of the CAB has been invoked to explain the differences in palaeoproxy records between sites in easternmost Africa (e.g. Lakes Tana and Challa) and those further to the west (e.g. Lake Tanganyika, Lake Victoria). This pattern appears to be a recurring feature of the geography of African palaeoclimate at both orbital and millennial scales. In these models, increased moisture availability to the sites in the west occurs via either enhanced convergence at the CAB (Tierney et al., 2011a, 2011b) or through its progressive influence on lacustrine basins as the CAB migrates east with the northerly migration of the ITCZ during peaks in boreal summer insolation (Costa et al., 2014). The Ethiopian and Kenyan highlands serve to isolate the easternmost sector of tropical Africa from the influence of the Atlantic Ocean (Verschuren et al., 2009; Tierney et al., 2011b). Sites in easternmost Africa respond instead to changes in the degree of moisture advected from the western Indian Ocean either via the northeast or southeast monsoons or sometimes both e.g. Lake Challa (Fig. 4), where palaeodata suggest increased rainfall at half-precessional dynamics (Verschuren et al., 2009).

2.4. Indian Ocean SST control on southern African rainfall

A suite of emerging palaeoecological data from southeast Africa has led researchers to reject a simple model of asymmetric hydroclimate change. Some authors advocate various degrees of expansion and contraction of the Winter Rainfall Zone (WRZ, Fig. 2) and strengthening and northward migration of the westerlies carrying Atlantic derived moisture (Chase and Meadows, 2007; Cockcroft et al., 1987; Stuut et al., 2002a; van Zinderen Bakker, 1976). This mechanism is ultimately driven by variability in the pole-equator temperature gradient and dominantly paced by glacial/interglacial cycles. Debate is ongoing as to the amplitude and/or geographical extent of that shift both northwards and eastwards (Chase et al., 2010; Heine, 1982; Shi et al., 2001; Stuut et al., 2004).

Under modern day conditions, SSTs (sea surface temperatures) in the Indian Ocean exert significant control on rainfall variability across the region affected by summer season rainfall (Jury et al., 1993; Reason and Mulenga, 1999). Indian Ocean SST variability over the Quaternary has been frequently cited as a driving mechanism for fluctuating humidity resulting in vegetation and landscape change in Southern Africa both on the eastern coastal

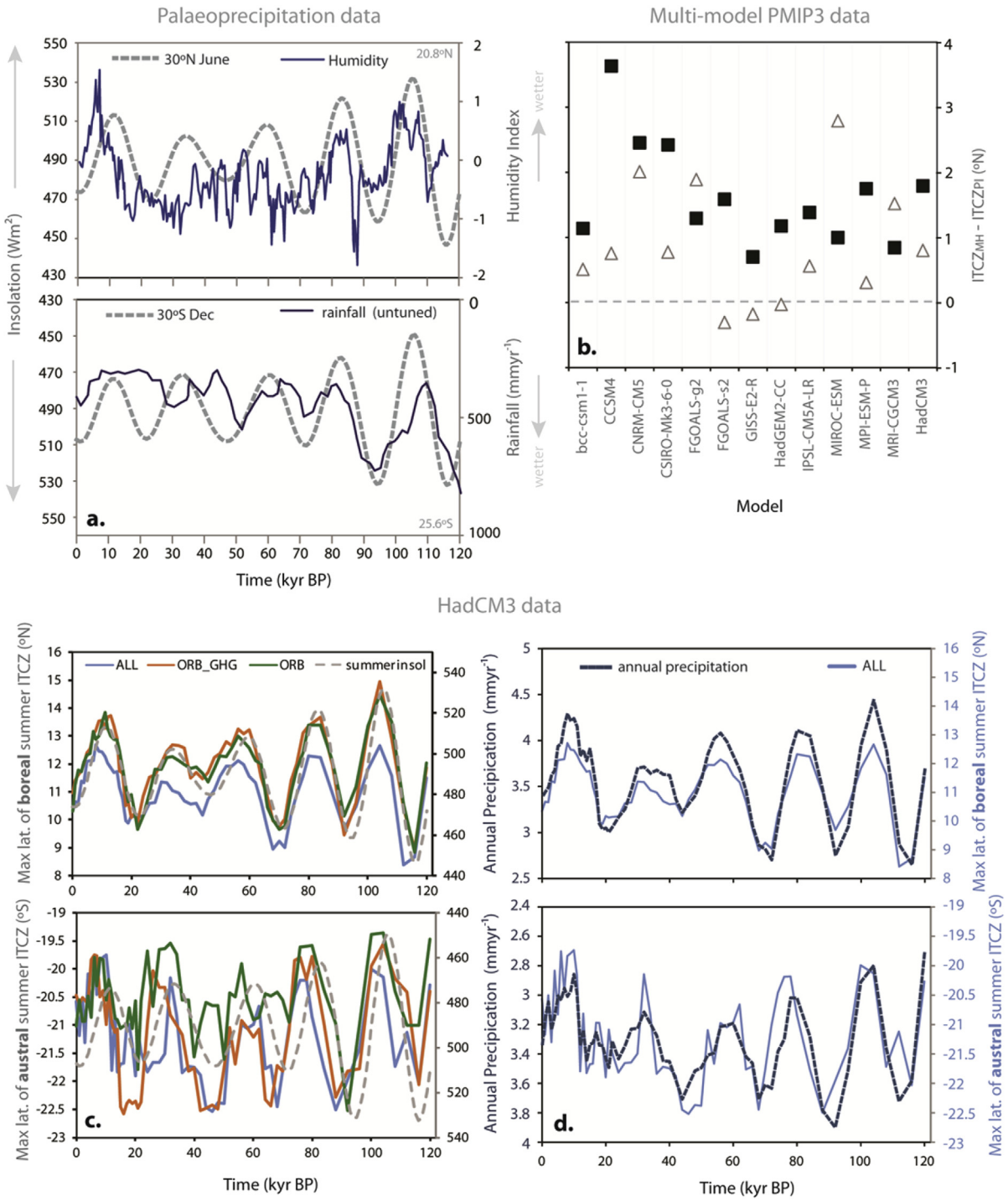

Fig. 3. a) Long time-series illustrating terrestrial palaeo-precipitation proxies from northern hemisphere Africa (top) (Tjallingii et al., 2008) and southern hemisphere Africa (bottom) (Partridge et al., 1997a) in relation to variations in their respective summer-season insolation (grey dashed line) (Berger and Loutre, 1991); b) Difference in the maximum latitudinal extent of both northern (squares) and southern (triangles) hemisphere rainbelt between Mid-Holocene ($ITCZ_{MH}$) and Pre-Industrial ($ITCZ_{PI}$) conditions for different models; c) Maximum latitudinal limit of boreal (top) and austral (bottom) summer rainbelt HadCM3 model simulation forced by variations in orbit only (ORB), greenhouse gases and orbital variations (ORB_GHG) and greenhouse gases, orbital and ice-sheet variations (ALL), variations in summer insolation (June average for boreal summer and December for austral summer) are given in the grey dotted lines in Wm^{-2}, values on the right-hand axes; d) Mean Annual Precipitation (MAP) for northern and southern hemisphere Africa simulated by HadCM3 (latitudinal extent from c is shown for comparison).

margins (Dupont et al., 2011) and further inland (Stokes et al., 1997; Truc et al., 2013). This model implies there is a strong positive correlation between southwest Indian Ocean SSTs and the intensity of southeast African rainfall via enhancing the availability of atmospheric moisture and that this, rather than direct insolation forcing, exerts first order control on hydroclimate variability in Southern Africa. SSTs in the Atlantic Ocean may also be important. Using dated dune records as a proxy for aridity, Stokes et al. (1997) suggested it was the SST gradient across southern Africa that was key to understanding past hydroclimatic change. Kalahari wet

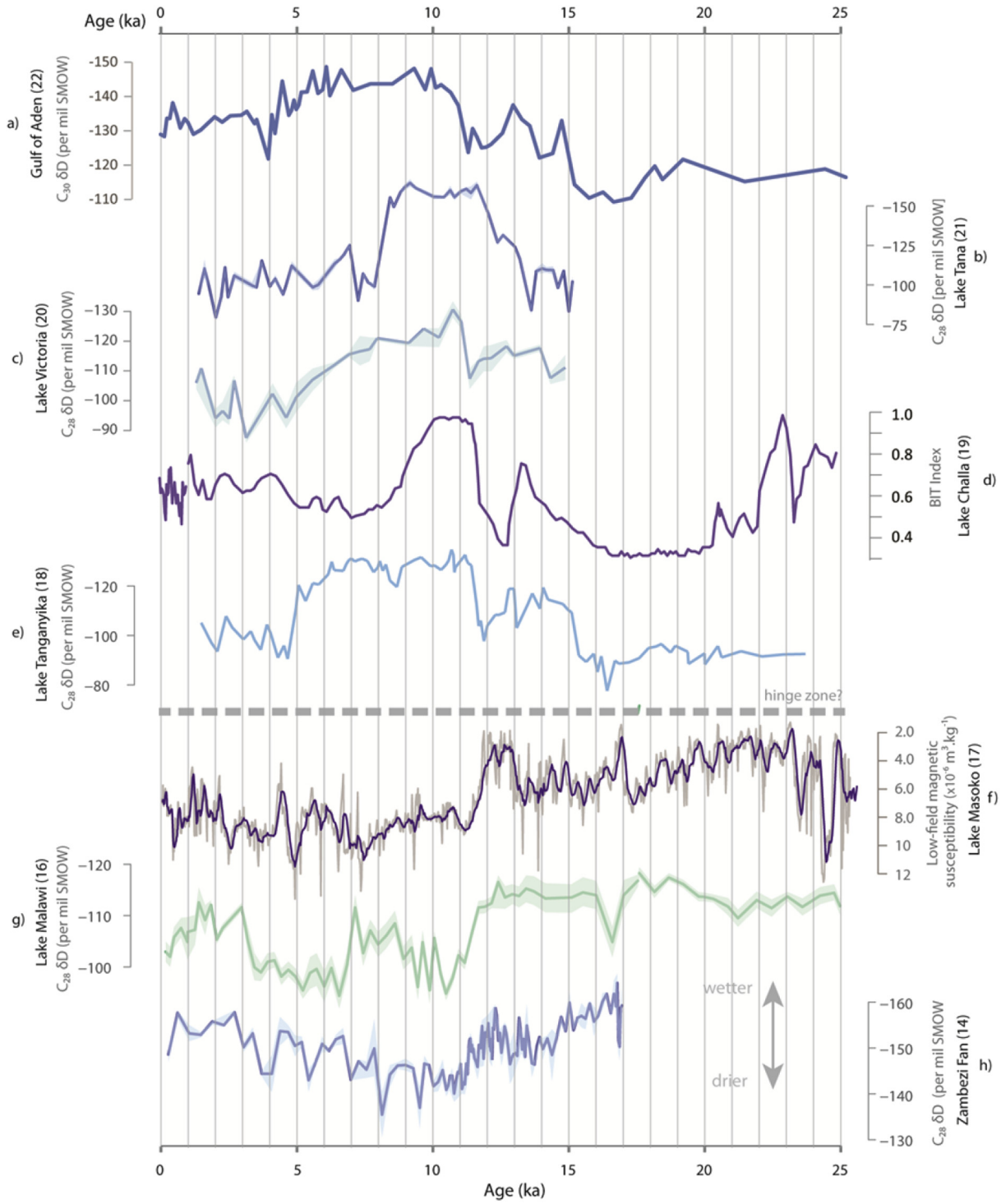

Fig. 4. East African palaeorainfall proxy time series: a) Gulf of Aden δD_{wax} (‰) (Tierney and deMenocal, 2013); b) Lake Tana δD_{wax} (‰) (Costa et al., 2014); c) Victoria δD_{wax} (‰) (Berke et al., 2012); d) Challa BIT index (Verschuren et al., 2009); e) Tanganyika δD_{wax} (‰) (Tierney et al., 2008); f) Lake Masoko magnetic susceptibility records (Garcin et al., 2006); g) Malawi δD_{wax} (‰) (Konecky et al., 2011); and h) Zambezi Fan δD_{wax} (‰) (Schefuβ et al., 2011).

phases were, it was argued, forced by large SST gradients which lead to stationary easterly disturbances over the African landmass and westward retreat of the South Atlantic anticyclone (Stokes et al., 1997).

These broad theoretical models are frequently offered up as mutually exclusive possibilities for governing past patterns of rainfall. The emerging suite of palaeodata across the continent, however, suggests that the dominance of a particular forcing mechanism is not only regionally inhomogeneous but has changed over time at any one site. The lower continental area of southern Africa and the co-occurring influence of both the Atlantic and Indian Oceans on hydroclimate change mean that a complex geographical pattern of past precipitation is more likely there than in northern Africa.

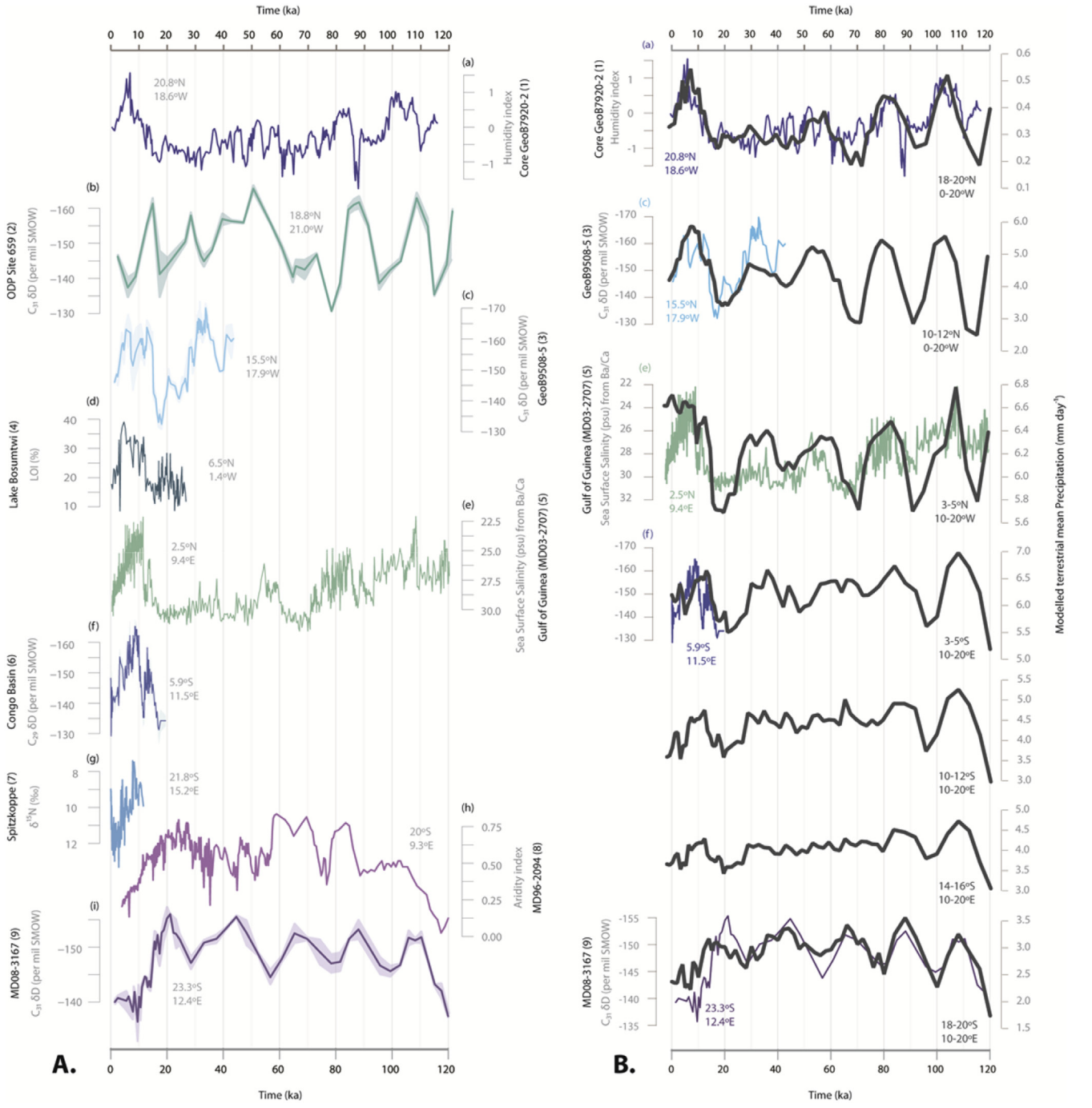

Fig. 5. A) West African proxy palaeorainfall records a) Grain-size derived continental humidity index from an ocean core offshore Mauritania (Tjallingii et al., 2008); b) C_{31} δD rainfall record from terrestrially derived sediments of the Saharan/Sahel region (Kuechler et al., 2013); c) Ocean core C_{31} δD rainfall record from terrestrial sediments derived from the western Sahel (Niedermeyer et al., 2010); d) Lake Bosumtwi sediment organic content derived from Loss on Ignition (LOI) (Peck et al., 2004); e) Gulf of Guinea sea surface salinity record controlled by freshwater input from the Sanaga and Niger Rivers (Weldeab et al., 2007); f) C_{29} δDwax rainfall record from the Congo basin (Schefuß et al., 2005); g) Hyrax midden $\delta^{15}N$ reflecting rainfall in the Northwest Namib (Chase et al., 2009); h) Walvis ridge southwestern Africa aridity index derived from grain size end-member modelling (ratio of aeolian end members to hemipelagic component) (Stuut et al., 2002b); i) C_{28} δD eastern Namib/western Kalahari rainfall record (Collins et al., 2014). Numbers in brackets refer to Table 1 and Fig. 2. B) Model simulated terrestrial precipitation (mm day^{-1}) for varying latitudes and longitudes. Proxy data from nearest palaeodata record (within 5° latitude) to modelled data shown on same plot for comparison.

3. Modelling methodologies

Model-data comparisons described in this study are primarily performed with a unique, existing set of palaeoclimate simulations over the last 120 kyr (originally described in Singarayer and Valdes, 2010) using the Hadley Centre coupled climate model, HadCM3. However, given that climate models may vary in their response to multi-millennial forcing due to differences in spatial resolution, model physics, and parameterizations, we examine the robustness of HadCM3 using multi-model outputs from the Paleoclimate Model Intercomparison Project (PMIP3) for the mid-Holocene and LGM. This enables us to elucidate common model responses to

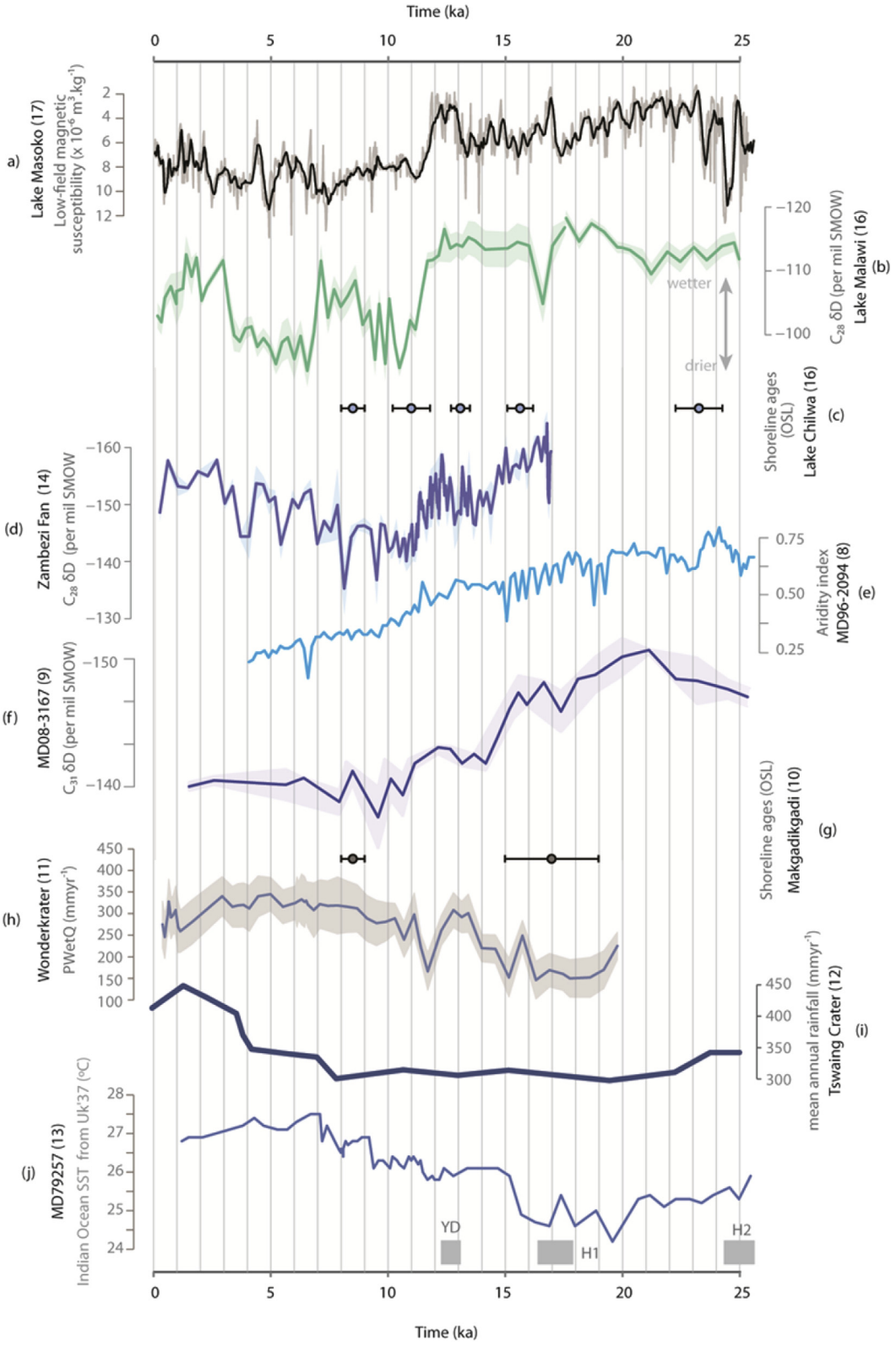

Fig. 6. Southern African palaeorainfall proxies a) Lake Masoko low-field magnetic susceptibility (lower values indicative of lower seasonal fluctuations and/or lake highstands) (Garcin et al., 2006); b) C_{28} δD record from Lake Malawi sediments (influenced by both moisture transport history and monsoon intensity) (Konecky et al., 2011); c) Shoreline ages at Lake Chilwa (dated highstands) (Thomas et al., 2009); d) C_{28} δD Zambezi basin rainfall record from the Zambezi Fan (Schefuß et al., 2011); e) Walvis Ridge sediment size aridity index (Stuut et al., 2004) f) C_{28} δD eastern Namib/western Kalahari rainfall record (Collins et al., 2014); g) Makgadikgadi shoreline OSL ages (Burrough et al., 2009a); h) Pollen derived wet season rainfall record from Wonderkrater (Truc et al., 2013); i) Tswaing crater rainfall record derived from sediment composition (Partridge et al., 1997a); j) Indian Ocean alkenone SST record (Bard et al., 1997; Sonzogni et al., 1998). Numbers in brackets refer to Table 1 and Fig. 2.

orbital and glacial forcing, and to outline regions of model disagreement where additional palaeodata may be useful for model evaluation. The models and experiments used are outlined in the following subsections.

3.1. HadCM3 glacial cycle simulations

HadCM3 is a GCM (General Circulation Model) consisting of coupled atmospheric, ocean and sea-ice model components, (Pope et al., 2000; Gordon et al., 2000) and in this study there is an additional coupled dynamic vegetation component. The resolution of the atmospheric model is 2.5° in latitude by 3.75° in longitude by 19 unequally spaced vertical levels. The spatial resolution over the ocean in HadCM3 is 1.25° by 1.25° by 20 unequally spaced layers in the ocean extending to a depth of 5200 m. The model contains a typical range of parameterizations in the atmosphere and ocean, including a detailed radiation scheme that can represent the effects of minor trace gases (Edwards and Slingo, 1996). The ocean model uses the Gent–McWilliams mixing scheme (Gent and McWilliams, 1990). The sea ice model is a simple thermodynamic scheme and contains parameterizations of ice drift based on surface ocean currents (Cattle and Crossley, 1995). The model version used here incorporates the MOSES2.1 land surface scheme (Essery et al., 2001) and the TRIFFID vegetation model (Cox, 2001), which divide the land surface into nine surface types, including five plant functional types. The land surface exchanges water, carbon, and energy with the atmosphere component. TRIFFID was asynchronously coupled in 'equilibrium mode' to speed up the time to reach steady state, i.e. the vegetation model was run for 50 years after every 5 years of climate model time.

HadCM3 is forced with prescribed changes in orbit (altering the seasonal and latitudinal distribution of solar insolation), greenhouse gases, sea level, and ice-sheet evolution (Fig. 7). Orbital parameters are taken from Berger and Loutre (1991). Atmospheric concentrations of CO_2 were taken from Vostok (Petit et al., 1999; Loulergue et al., 2008) and CH_4, and N_2O were taken from EPICA (Spahni et al., 2005), with all data transferred to the EDC3 timescale (Parrenin et al., 2007). Ice-sheet reconstructions use the ICE5G model of Peltier (2004) for pre-industrial to LGM time slices, which includes a detailed evolution of the ice thickness, extent, and isostatic rebound for the last 21 kyr. This dataset was used to calculate GCM continental elevation, bathymetry, ice area, and land-sea mask using an anomaly-based method for consistency with the HadCM3 pre-industrial boundary conditions. Prior to the LGM, when ice-sheet extent is relatively unconstrained, the ice extent and height producing a particular ice volume for pre-industrial to LGM were mapped onto similar ice volumes for LGM to 120 kyr BP, as given by SPECMAP global sea level curve (see Singarayer and Valdes, 2010; and Eriksson et al., 2012 for model details).

Three sets of snapshot simulations have been run (see also Singarayer et al., 2011), each consisting of 62 model runs covering the whole of the last 120 kyr. In the first set of simulations, **ORB-ONLY**, only the orbital configuration was modified for each time slice, with all other boundary conditions set to pre-industrial. In the second experiment, **ORB + GHG**, orbit and trace greenhouse gases were modified. In the final experiment, **ALL**, additional boundary conditions of ice-sheet extent/height and sea level were included. In all simulations the initial conditions were the same, based on a prior spun-up pre-industrial simulation, and each was run to equilibrium for 500 years. The climatologies presented here are averages of the last 30 years. See Fig. S2 for the pre-industrial seasonal variation in rainfall and 10 m winds as simulated by HadCM3 over Africa.

This modelling methodology focuses on multi-millennial scale variations in hydroclimate and does not include millennial-scale

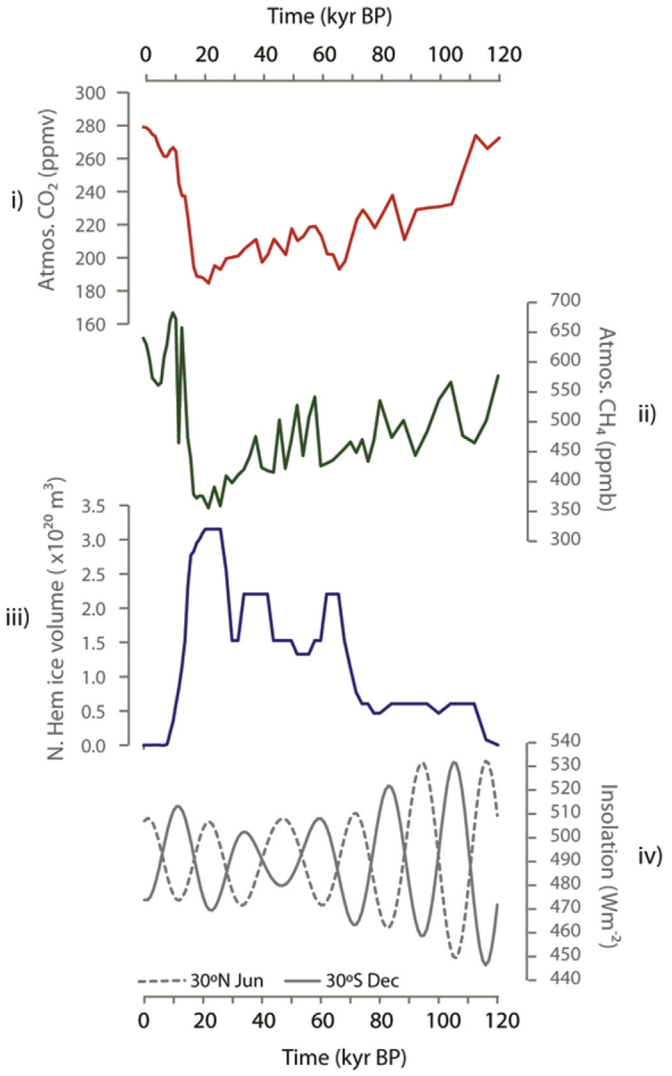

Fig. 7. HadCM3 model inputs. From top to bottom: i) Global Atmospheric CO_2 (Petit et al., 1999); ii) global Atmospheric CH_4 (Spahni et al., 2005); iii) Northern Hemisphere ice-sheet volume (Peltier, 2004); iv) variability of insolation at the earth's surface over time (Berger and Loutre, 1991).

variability such as Dansgaard-Oeschger events and Heinrich events, although relevant Heinrich event simulations are in existence (Singarayer and Valdes, 2010). A second qualification is that the methodology assumes the climate is in equilibrium with the boundary conditions and is not affected by initial conditions (i.e. there are not multiple possible stable states). Previous publications using these and related model simulations suggest this is a reasonable first order approximation for multi-millennial climate variability (e.g. Singarayer and Valdes, 2010; Singarayer et al., 2011).

All time slices over the last 120 kyr were examined for all three HadCM3 experiments to assess the most important factors driving variation in the position and seasonal range, as well as the symmetry/asymmetry of the rainbelt in the model for comparison with the palaeorecord (e.g. Partridge et al., 1997).

3.2. PMIP3 simulations

The HadCM3 experiments covering the last glacial cycle are complemented by model simulations from a range of coupled models run as part of the CMIP5/PMIP3 initiatives (downloaded from http://cmip-pcmdi.llnl.gov/cmip5/dataportal.html in Mar

2014). At the time of downloading there were 13 models for which pre-industrial and mid-Holocene (6 kyr BP) conditions are available and 8 models for which a Last Glacial Maximum (LGM) simulation was performed. See Table 2 for details of those models for which palaeo time slices were available. The mid-Holocene simulations included changes to orbital configuration and greenhouse gases for 6 kyr BP. We have used the HadGEM2-CC model output in the results sections but not the HadGEM2-ES version due to the short length of integration available with the latter model version for the mid-Holocene. The LGM simulations included changes to orbital configuration and greenhouse gases appropriate to 21 kyr BP, and ice-sheet related changes to orography using ICE6G. Taylor et al. (2012) and Braconnot et al. (2012) provide further details of the CMI5/PMIP3 experimental set-up. There are minor differences in the boundary conditions used for mid-Holocene and LGM boundary conditions between the PMIP3 simulations and the HadCM3 simulations described in section 3.1, e.g. use of ICE5G with HadCM3 vs. ICE6G for PMIP3. However, these are small enough to enable reasonable comparison of the two sets of experiments at the relevant time slices.

3.3. Calculating variations in the inter-hemispheric latitudinal range of the tropical rainbelt

To calculate the seasonal latitudinal range of the tropical rainbelt we follow the approach of Braconnot et al. (2007) to find the latitudes encompassing the core of the rainbelt. To find the northern limit of the core rainbelt, for each longitude, the latitudinal position of weighted monthly mean precipitation on the north side of peak precipitation for that month was calculated. This enables any spurious precipitation in arid regions to be disregarded to obtain a more robust estimate of the tropical rainbelt than taking the absolute northern limit of precipitation. Braconnot et al. (2007) used this method for the northern hemisphere alone, but here the method is similarly used in the southern hemisphere to find the total latitudinal range of the rainbelt. At any longitude, the maximum seasonal rainbelt excursion north or south is given by calculating the maximum North/South latitude over all months (i.e. the timing of the seasonal extremes is allowed to vary by this method).

4. Results

4.1. Interhemispheric variations in rainbelt seasonal range

As found previously, the model suggests that the extent of the northern excursion of the African rainbelt (Fig. 3c) in boreal summer varies in phase with northern hemisphere summer insolation (e.g. Braconnot et al., 2007; Marzin and Braconnot, 2009; Kutzbach et al., 2008). Similarly, the maximum southern excursion of the austral summer rainbelt (Fig. 3c) varies in phase with southern hemisphere summer insolation. In combination, the model tropical African rainbelt range shifts latitudinally in response to orbitally driven variation in seasonal insolation, and corroborates earlier assertions based on palaeoenvironmental data (e.g. Partridge et al., 1997, Schefuß et al., 2011; Collins et al., 2014, Fig. 3a).

Comparison of all three model experiments (ORB-ONLY, ORB + GHG, ALL) reveals that the largest variations in latitudinal position of the rainbelt result from orbital configuration insolation, with secondary impacts from changes to greenhouse gases (GHGs) and ice-sheets/sea level (Fig. 3c), although a proper factor separation is not possible in this experimental set up without further experiments to isolate all the forcings in turn. Both GHGs and ice-sheets (in conjunction with orbital forcing) produce asymmetric responses; with ice-sheet expansion occurring mostly in the northern hemisphere, and reduced GHGs in the glacial producing cooling that was larger in the northern hemisphere due to the larger area of land there compared to the southern hemisphere. In order to compensate for the larger cooling in the northern hemisphere, resulting from continental ice-sheet expansion and GHG reductions during the last glacial period, the model rainbelt moves south to scavenge heat from the warmer hemisphere (mechanism described in Broccoli et al., 2006). This can be seen by comparison of the three curves in Fig. 3c. The modelled boreal summer northern rainbelt limit is more sensitive to ice-sheet changes and the southern limit more sensitive to GHGs (Otto-Bliesner et al., 2014; found similar sensitivity of the southern African tropics to GHGs). However, both forcings also produce asymmetric variations in the rainbelt.

Similar calculations for the mid-Holocene (MH) vs. Pre-Industrial (PI) time slices with available PMIP3 model outputs demonstrate that this asymmetric response to the orbitally driven changes in insolation seasonality is a robust response (Fig. 3b). All models produce northward movement of the northern limit of the boreal summer rainbelt in the MH in response to enhanced boreal summer insolation (replicating the results from Braconnot et al., 2007 with PMIP1/PMIP2 models). However they generally underestimate the magnitude of increase in precipitation in comparison with palaeodata syntheses (Bartlein et al., 2011; Pérez Sanz et al., 2014; Braconnot et al., 2012). There is less agreement in the southern hemisphere limit, but 10 of 13 models agreed with the results produced by the HadCM3 experiment. This is despite the precipitation anomalies (MH-PI) being much more spatially

Table 2
List of CMIP5/PMIP3 models and available palaeoclimate simulations. OA refers to coupled ocean-atmosphere models. OAC refers to coupled ocean-atmosphere-carbon/vegetation models.

Model	Atmos. Res.	Model config.	Available simulations			Reference
			PI	MH	LGM	
bcc-csm1-1	128 × 64 × L26	OAC	Y	Y		Wu et al. (2013)
CCSM4	288 × 192 × L26	OA	Y	Y	Y	Gent et al. (2011)
CNRM-CM5	256 × 128 × L31	OA	Y	Y	Y	Voldoire et al. (2013)
CSIRO-Mk3-6-0	192 × 96 × L18	OA	Y	Y		Rotstayn et al. (2010)
FGOALS-g2	128 × 60 × L26	OA	Y	Y	Y	Li et al. (2013)
FGOALS-s2	128 × 108 × L26	OA	Y	Y		Bao et al. (2013)
GISS-E2-R	144 × 90 × L40	OA	Y	Y	Y	Schmidt et al. (2014)
HadGEM2-CC	192 × 145 × L60	OAC	Y	Y		Collins et al. (2011)
HadGEM2-ES	192 × 145 × L38	OAC	Y	Y		Collins et al. (2011)
IPSL-CM5A-LR	96 × 96 × L39	OAC	Y	Y	Y	Dufresne et al. (2013)
MIROC-ESM	128 × 64 × L80	OAC	Y	Y	Y	Watanabe et al. (2011)
MPI-ESM-P	192 × 96 × L47	OA	Y	Y	Y	Jungclaus et al. (2006)
MRI-CGCM3	320 × 160 × L48	OA	Y	Y	Y	Yukimoto et al. (2011)

variable in the southern hemisphere than the northern (see Fig. 8 for PMIP3 models HadCM3). There was no common pattern to the inter-model magnitude of N/S response. In other words, models with large movement of the northern rainbelt excursion did not necessarily have a larger southern excursion.

While the boreal summer rainbelt variations strongly correlate with precession-dominated boreal summer insolation throughout the modelled last 120 kyr, the southern rainbelt displays a greater degree of noise and has generally lower correlation with austral summer insolation from ~50 kyr to PI (Fig. 3c) than the northern hemisphere rainbelt has with boreal summer insolation. During this period, precessional insolation variation has been muted compared to the earlier half of the last glacial cycle, due to reduced eccentricity modulation (Fig. S1). When insolation is a smaller driver, the lower continentality of southern Africa results in more influence from internal climate variability than in northern Africa in HadCM3. Given the short length of the climate averages (30 yr) it appears that multi-decadal variability in rainbelt position has a similar magnitude as its response to insolation, resulting in a relatively noisy time series (in particular for ORB-ONLY, Fig. 3c). Extrapolation from the modelled result would suggest that when precession-driven insolation variation is small, other driving forces might dominate the palaeo-precipitation signal in southern African data more so than has similarly been observed in northern Africa (Kuechler et al., 2013; Tjallingii et al., 2008).

Results from HadCM3 for the African rainbelt asymmetry (Fig. 3c/d) are consistent with key palaeodata findings (Collins et al., 2014; Partridge et al., 1997a; Schefuß et al., 2011). However, it is important to acknowledge the care that must be taken in interpreting palaeo-precipitation records from single sites in terms of movement in the rainbelt. It is not possible to distinguish changes in the rainbelt position from changes in rainbelt intensity of precipitation from a single location, rather data from a range of latitudes must be compiled (Shanahan et al., 2015). Even then interpretation can be difficult since changes in intensity and rainbelt shifts do not necessarily co-vary in all geographical locations, and may even vary out of phase in certain areas (Singarayer and Valdes, in review). However, in the particular case of northern and southern Africa, the annual mean precipitation near the seasonal limits of the tropical rainbelt does echo the rainbelt shifts in this model (Fig. 3d).

Of equal note is the behaviour of the rainbelt in any one season in response to insolation forcing. The simple picture of latitudinal shifts in the whole precipitation band does not apply when considering individual seasons. When insolation increases (decreases) in any month, the precipitation increases (decreases) over a wide latitudinal range (for non-coastal regions), resulting in pulses of higher (lower) rainfall also to the north and south in the main rain band at these times (Fig. 9). Similar responses can be seen in the majority of the PMIP3 models' monthly/seasonal precipitation. This is in contrast to the variation in convergence (ITCZ) near the surface (Fig. S3), which primarily shifts meridionally, especially over northern Africa. Due to relatively small thermal inertia over land (in comparison with oceans) local surface heating dominates the response in the continental interior (Chiang and Bitz, 2005), resulting in higher rainfall over a wide latitudinal range.

4.2. Spatial patterns in the equatorial response

Recent palaeodata retrieved from lower latitudes and mainly from the western African continent or offshore sediment cores from the west coast suggest a coherent response in the northern and southern hemispheres (e.g. Collins et al., 2011, Fig. 5A). At first glance this result seems at odds with prior findings of asymmetric shifts in the latitudinal range of the rainbelt (Fig. 3). The expectation might be for similar asymmetric trends in the northern and southern regions of equatorial Africa. Using the HadCM3 suite of simulations covering the last glacial cycle it is possible to examine

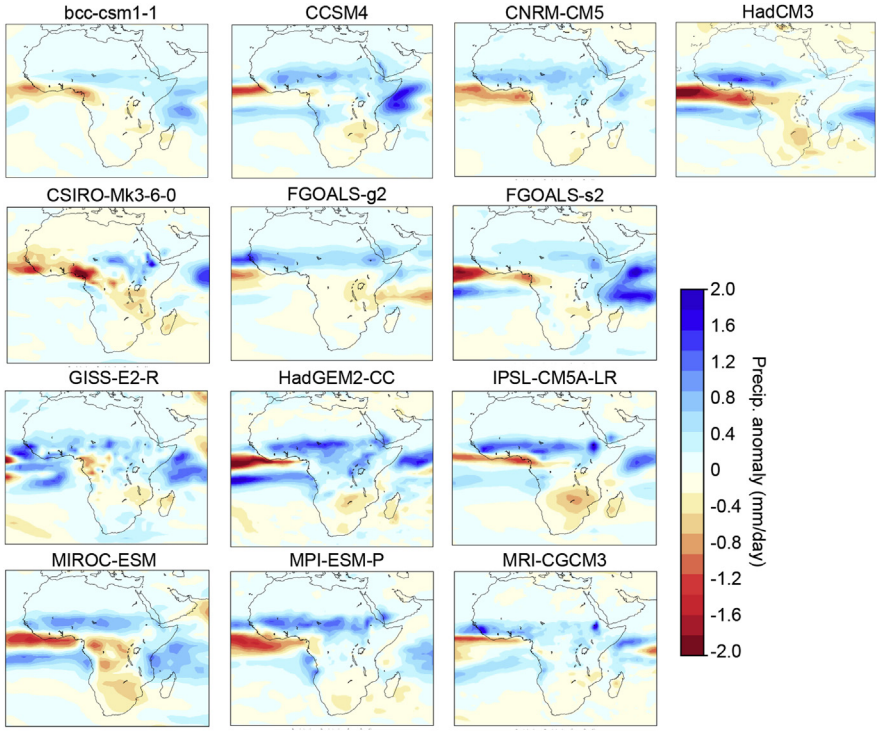

Fig. 8. Mid-Holocene minus Pre-industrial mean annual precipitation anomalies (in mm/day) of the available models from the PMIP3 experiment. See Table 2 for individual model details.

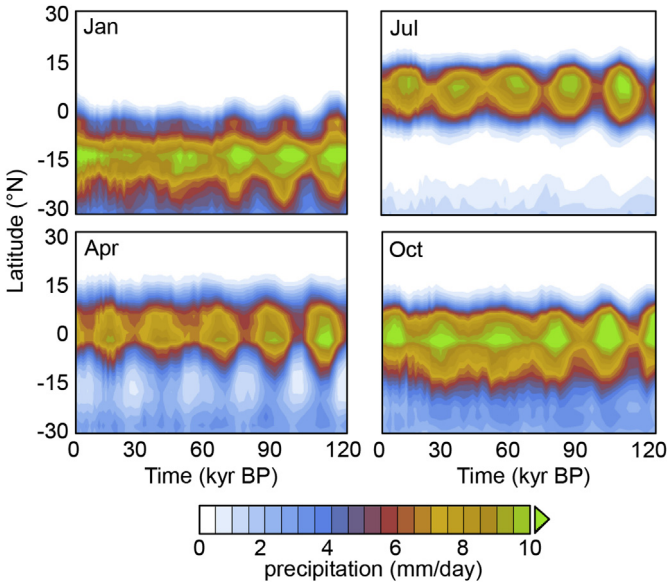

Fig. 9. Changes in January, April, June and October precipitation for latitudes between 30°S and 30°N over the last glacial cycle in the HadCM3 'ALL' experiment averaged over 15–30°E.

this by recreating equivalent model-based latitudinal time series (Fig. 5B) to those collated in the palaeorecords, which in general reflect changes in past rainfall, and in the case of offshore cores, integrate a region of around ten degrees inland from the coast (cf. source regions for offshore cores in Fig. 2).

For the ALL experiment, time series of annual precipitation at numerous latitudinal locations on the west side of Africa between 20°N and 16°S all demonstrate ~20-kyr cyclicity (Fig. 5B). At these latitudes (except 3–5°N of Fig. 5B) a general drying is simulated over the Holocene, following a wetter early Holocene and an LGM that was as dry as the PI or drier. This reflects the pattern observed in available palaeodata (Fig. 5A), and at a coarse temporal resolution could be considered approximately symmetric. At the most southern latitude plotted (18–20°S; Fig. 5B) the sense of symmetry breaks down somewhat in the model. Here, the drying begins even earlier near the LGM and then remains relatively dry from the mid-Holocene onwards (as also seen in the data).

The apparent 'symmetry' in wet/dry phases around the equator between 20°N and 16°S is more complex when considered in more detail. The southern-latitude model output for West Africa effectively leads the northern hemisphere by 3–5 kyr throughout the glacial cycle. At these southern equatorial latitudes the majority of annual precipitation falls between September to May, but is essentially bimodel, with two peaks at roughly November and March/April (varies with time slice; Fig. S4). Given this seasonality, one might expect the annual mean precipitation to follow Jan/Feb insolation (somewhere in the middle of the rainy season). However, the model rainfall here effectively has a temporal variation equivalent of following May insolation. In the earlier part of the rainy season (Oct–Feb) the precipitation is in *anti-phase* with local insolation (for reasons explained in the next paragraph). However, in the later part of the rainy season (Mar–May) the precipitation is *in phase* with local insolation. The superposition of these two phases results in the overall annual precipitation being roughly in phase with May insolation (see Fig. S4), resulting in an apparent lead of 3–5 kyr over the northern latitudes (which are in phase with July/August insolation).

The anti-phasing of Oct–Feb precipitation with local insolation originates in the dynamic ocean response to changes in seasonal insolation. The HadCM3 Atlantic ITCZ responds to interhemispheric temperature gradients by shifting to the warmer hemisphere to scavenge heat (Broccoli et al., 2006; Chiang and Bitz, 2005). When boreal summer insolation is high the northern hemisphere warms more than the southern hemisphere due to the larger continental area in that hemisphere, which has smaller thermal inertia than ocean. This results in lower precipitation at the equator and higher precipitation to the north over the Atlantic. When boreal summer insolation is high, coincident austral summer insolation (and boreal winter insolation) is low. As a result, the northern hemisphere cools more than the southern hemisphere (again due to higher continentality) and consequently the austral summer Atlantic ITCZ shifts into the warmer southern hemisphere to compensate. Its impact on annual rainbelt precipitation over the Atlantic is to create wetter conditions to the north and south of the equator and drier conditions close to the equator, i.e. symmetric expansion (contraction) of the oceanic rainbelt when boreal summer insolation is at a maximum (minimum) (Singarayer and Valdes, in review). This oceanic feature is a robust characteristic observed in HadCM3 and the majority of PMIP3 models (Fig. 8). In HadCM3 the precipitation anomalies originating in the tropical Atlantic are advected into west coast regions of Africa, resulting in roughly latitudinally symmetric variation in precipitation during October to February. However, by the peak rains between March and May the impact of local insolation on temperatures over southwest tropical Africa predominates the precipitation response (because the relative impact of local convection over land increases) and so the rain in these months follows local seasonal insolation rather than being in anti-phase.

In HadCM3 model output, there is a small latitudinal band of simulated drier conditions at the equator on the west coast when wetter conditions prevail to the north and south (Fig. 8). However, there is a high level of inter-model variation in the extent to which the latitudinal 'wetter-drier-wetter' spatial pattern of Atlantic anomalies is advected over coastal regions to the continental interior (Fig. 8). For example, CCSM4, FGOALS-s2, IPSL, and MPI models display features in spatial patterns in MH-PI annual mean precipitation anomalies along the western side of Africa that are similar to HadCM3. However, in HadGEM2-CC the drier equatorial Atlantic anomalies do not propagate significantly onto the continent, resulting in predominantly wetter conditions over the whole latitudinal range between 20°S and 20°N. In MIROC and FGOALS-g2 model output the wetter southern Atlantic conditions during the MH are mostly/entirely restricted to the ocean, and this results in an N–S dipole response over the continent with drier conditions south of the equator and wetter conditions in the northern hemisphere.

The differences between models will be a consequence of different land-atmosphere coupling strengths, differences in included processes, inconsistent boundary conditions (Braconnot et al., 2007), parameterizations relating to convection, and spatial resolution. Further work is required to assess which factors dominate the inter-model variation. However, this northern equatorial region has the potential to differentiate model skill in tropical hydroclimate using palaeodata. Comparison of the model data with the palaeodata (Fig. 5B) highlights a significant disagreement in the direction of change during the Holocene (at 3–5°N). In the model, the latitude of the switch from wetter to drier equatorial conditions due to precessional-scale forcing moves southwards during the glacial in response to hemispherically asymmetric ice-sheet forcing, so that during the glacial period this particular region sits slightly more within the 'wetter' northern regime when boreal summer insolation is high, but during the Holocene it has a higher proportion of area in the 'drier' equatorial regime when summer insolation is high. The available palaeodata do not seem to suggest

such a change in regime at this latitude. This might reflect the more northern location of the catchment region of the fluvial systems that feed the Ocean Core in the Gulf of Guinea (site 5, Fig. 2) which reflect a wetter Saharan/Sahel region, or that HadCM3 is expressing this mode of variation at the wrong latitudes and/or overestimating the advection of this oceanic pattern over terrestrial regions. Palaeodata that directly reflects terrestrial hydrological change at these equatorial latitudes would greatly improve our ability to assess the model outputs for this region.

Note that while our results suggest that multi-millennial orbital forcing can result in an element of symmetry between N and S on the west coast of Africa, Otto-Bliesner et al. (2014) also found a symmetrical response to millennial-scale forcing in a transient simulation of the last deglaciation. In their study the symmetrical response in North Africa and southeast equatorial Africa occurs following resumption of the Atlantic meridional overturning circulation. They find that the wetter conditions in their model in northern and southern Africa were responses to increases in GHGs, which in the northern hemisphere was amplified by coincident orbital configuration changes that also would produce wetter conditions.

4.3. Mechanisms of variation in East African rainfall

The development of δD_{wax} as a terrestrial proxy for past rainfall in the tropics and the subsequent emergence of new long δD_{wax} datasets has greatly contributed to the generation of hypotheses on the mechanisms of hydroclimate variability. The challenge of apportioning changes in δD_{wax} observed in large lake basins and ocean cores to either rainfall amount or moisture source region and transport history (Konecky et al., 2011; Costa et al., 2014) is now widely acknowledged and indeed is partially responsible for the recognition that changes in past rainfall go beyond simple models of increased/decreased mean annual precipitation and must also consider changing synoptic circulation patterns, complex interaction of different moisture sources, and the role of seasonality (e.g. Konecky et al., 2011; Verschuren et al., 2009; Costa et al., 2014). Variations in East African hydroclimate have recently been attributed to zonal circulation changes rather than direct meridional movement of the ITCZ (Tierney et al., 2011a; Costa et al., 2014). It has been proposed that changes in either the East-West position of the CAB (see Fig. 1) or in the intensity of convergence at the CAB are a primary factor influencing not only the magnitude of rainfall but also the proportion of moisture sourced from the Atlantic vs. Indian Oceans (Tierney et al., 2011a/b). The spatial pattern of hydroclimate variability on multi-millennial timescales indicates that the East African Rift System (EARS) topography also plays an important role in the East-West dipole pattern seen in palaeolake records of the region at various time periods by isolating the most easterly lakes from Atlantic moisture sources.

HadCM3 generally displays zonally divergent patterns within East Africa(Fig. 10). This is supported most clearly in the palaeodata at 21 ka where we broadly observe a pattern of wetter conditions to the east of the EARS and drier conditions prevailing to the west (Fig. 11c). Indeed HadCM3 displays much higher skill than other models in this regard (Fig. S8; see also DiNezio and Tierney, 2013). Palaeodata from lakes Nakuru and Challa are indicated as dry at 21 ka in contrast to the model output, though both basins exhibit a definitively wetter early LGM (25–22 ka) with a drying trend from 22 ka (Street-Perrot et al., 1989; Verschuren et al., 2009) and δD_{wax} records from the same basin suggest that for the majority of the LGM easternmost Africa was characterised by wetter conditions (Tierney et al.,. 2011). The location of the wet-dry divide in the model is further west than the palaeodata suggest, which is most likely due to relatively low spatial resolution of EARS topography in the model. The increase in rainfall over the easternmost sector originates in the Indian Ocean where there is an increase in convective activity. This is a result of exposure of the Sunda Shelf (due to lower sea level) in the Indo-Pacific (DiNezio and Tierney, 2013), which sets up a pattern of higher pressure in the Walker circulation over that region with associated uplift (see vertical velocity field, Fig. 11a) and increased precipitation over the western Indian Ocean (Fig. 11c). Further sensitivity experiments demonstrate that this response has primarily to do with sea level change but also to a smaller extent the direct climatological influence of ice-sheets (Roberts and Valdes pers. comm.). Changes in sea level throughout the glacial (~80 kyr–~12 kyr BP) contribute significantly to the variation in precipitation, resulting in a lower level of precessional variance compared to other tropical African regions during the glacial, although 23 kyr cyclicity is still evident (Fig. not shown). The generally wetter conditions towards coastal East Africa over this time frame are potentially reflected in several palaeolake records (Scholz et al., 2007; Moernaut et al., 2010). However, during MIS5 (120kyr–~80 kyr BP) and the Holocene precessional-related insolation changes are the main driver of E African hydroclimate variation in HadCM3.

The tropical zonal Walker Circulation anomalies govern East African precipitation variation through boreal autumn and winter seasons (see 21 kyr vs. PI seasonal precipitation in Fig. S5). Increased precipitation to the east of the EARS at the LGM (Fig. 11c) is the result of increased moisture advection from the Indian Ocean. However, there is a decrease in convergence over the CAB region (Fig. 11b) and westerly (i.e. directed offshore) 10 m wind anomalies (Fig. 11c). In other words, the winds transporting moisture from the Indian Ocean onto the continent are reduced but more highly moisture-laden because of increased convection occurring over the ocean.

More depleted δD_{wax} signals relative to the late Holocene (blue squares in Fig. 10) have also been attributed to a difference in moisture source as well as increased in rainfall amount. The degree to which either factor affects the δD_{wax} signal is highly site specific. In particular, it has been argued (based on multiple proxies) that the δD_{wax} signal from Lake Malawi is dominated by moisture source and transport history (Konecky et al., 2011) so that, for example, despite depleted δD_{wax} during the LGM, other palaeorecords suggest Lake Malawi was in fact moderately drier (Castaneda et al., 2007; Barker et al., 2007). In terms of response to insolation seasonality, when boreal summer insolation is higher, changes to water hydrogen isotope ratios (more strongly depleted in deuterium) have been tentatively linked to eastward movement of the CAB and increasing moisture derived from the Congo and other western sources, occurring in conjunction with northward movement of the ITCZ (Costa et al., 2014). In the early-to mid-Holocene the HadCM3 simulations produce generally wetter conditions over the EARS region and northern Africa in general (Fig. 10b and c) and drier conditions at the southern end of the EARS. This pattern approximately matches the palaeohydrological data (Figs. 4 and 10b).

The seasonality of East African precipitation in the model changes significantly with insolation. During the early and mid-Holocene simulated SON precipitation increases (potentially reflected in some palaeorecords [e.g. Barker et al., 2011]), and is the largest contributor to the annual mean while the contribution from DJF decreases (Fig. S7b and c), and around 12 kyr BP the highest rainfall occurs in MAM (see Fig. S7b and c). The SON increase in modelled precipitation in the early and mid-Holocene is due to eastward movement of the convergence zone (at the CAB; Fig. S2) in conjunction with northward movement in convergence at the ITCZ (Fig. S2), as speculated in previous studies (Costa et al., 2014).

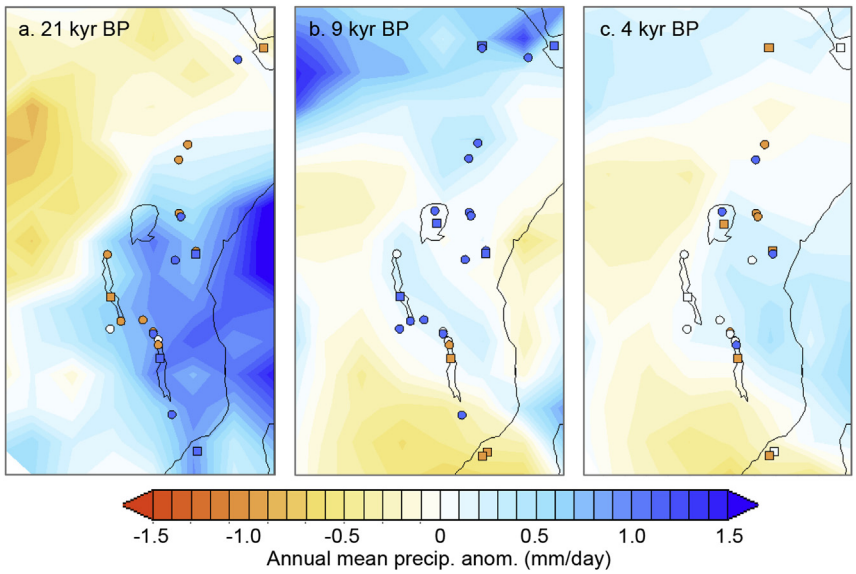

Fig. 10. HadCM3 mean annual precipitation anomalies (filled contours) from the ALL experiment for (a) 21 kyr BP, (b) 9 kyr BP, and (c) 4 kyr BP. Superimposed on the contours are palaeo-hydroclimate proxy data. Palaeo-records are displayed on the map as circles (palaeohydrological proxies) or squares ($\Delta\delta D_{wax}$ anomalies, which in some basins can also be strongly influenced by rainfall source). The colour for each record is categorical and is indicative of conditions that are drier (orange), wetter (blue) or have no change (white) from the late Holocene mean (0–2 ka) (see Table S1 for details of the palaeorecords used to construct these time slice plots). (For interpretation of the references to colour in this figure legend, the reader is referred to the web version of this article.)

It is a seasonal specific response in the model, which is manifest in the annual rainfall anomalies (Fig. 10b).

While the East African lakes region extends further south than the equator, there is a clear coherence in timing of wet-dry periods with the northern hemisphere (e.g. Fig. 4 for data, and Fig. 10 and Fig. S7 for the model). In light of this, a dominant influence of northern extratropical forcing on Indian Ocean temperatures rather than local insolation forcing of the rainbelt has been hypothesized as a key control (e.g. Tierney et al., 2008). It is certainly the case that remote forcing, related to northern high latitude changes (as discussed above), are important. However, in the model, the phase of the ~23-kyr cyclic variation in each month shows an important direct response to local insolation forcing. The east-west dipole in early Holocene response (Fig. 10b) is due to advection of drier equatorial air from the Atlantic as its rainbelt expands latitudinally at that time, producing a drier rainbelt core (as discussed in section 4.2). The easternmost part of the region is relatively isolated from this by the EARS, and as a consequence the western and eastern parts of East Africa are roughly in anti-phase in the model when precessional-insolation forcing is dominant. A similar contrasting pattern of rainfall in western and eastern parts of East Africa also occurs in the model at the LGM due to glacial sea level/ice-sheet changes, as described earlier in this section.

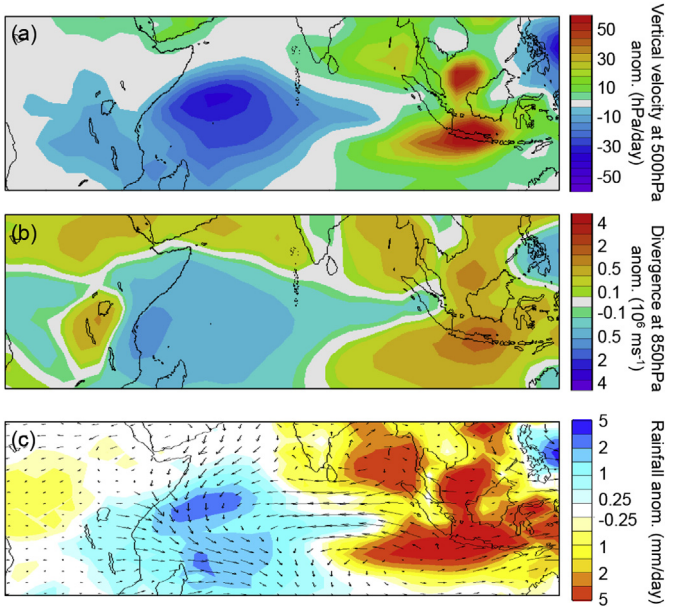

Fig. 11. East Africa LGM minus PI annual mean anomalies from the HadCM3 'ALL' experiment for (a) vertical component of velocity in the p-coordinate at 500 hPa, where negative values equate to rising air mass anomalies, (b) divergence at 850 hPa, and (c) rainfall.

Another result of the change in seasonality in East African hydroclimate is an asymmetric timing of peaks and troughs in rainfall throughout the glacial cycle. Additionally, a change in seasonality may alter the contribution from Atlantic and Indian Ocean moisture sources to local annual total rainfall, which would influence isotopic hydroclimate-proxies. The model results also imply that the idea of a 'hinge zone' (see section 2.1), separating locations with a northern mode of response from those with a southern mode, should be treated with caution as the location and nature of such a zone would most likely vary with time depending on the dominant forcing. For example, the HadCM3 MH anomalies in annual mean precipitation (Fig. S7) suggest a north-south divide occurring over the Lake Malawi region and previous model simulations of Heinrich events suggest a similar hinge zone for millennial-scale northern high latitude forcing (Thomas et al., 2009). However, the model LGM anomalies show all eastern lakes responding in concert (Fig. 10a), suggesting a hinge zone further towards the northern lakes (near Lake Turkana). This is also another region where the PMIP3 models display large inter-model variation in the location/existence of a hinge zone (Fig. 8 and Fig. S6). Previously, palaeodata records suggested Lake Malawi lake levels were high during the LGM (Johnson, 1996; Finney et al., 1996) but more recent data strongly suggests a moderate dry period (Gasse et al., 2002; Johnson et al., 2002; Castanada et al., 2007). Close by, independent palaeodata from Lake Masoko have also provided opposing interpretations for both a drier (Barker et al., 2003) and

wetter (Garcin et al., 2006) LGM (Fig. 10b, Table S1). The proximity of the 'hinge zone' to these basins and its movement over time may go some way to explaining the disparity in these palaeodata.

4.4. Correlations between sea surface temperature and precipitation

Lastly, we use the model simulations to examine the idea that for some regions sea surface temperatures (SSTs) primarily drove hydroclimate and vegetation changes, evidenced by positive correlations between regional SST proxies and terrestrial reconstructions of vegetation (Dupont et al., 2011) or rainfall (Truc et al., 2013). HadCM3 results demonstrate correlations that are regionally and temporally variable as the dominance of driving factors changes through the glacial cycle. As an illustration, East African annual mean precipitation is positively correlated with SSTs when forced with orbital insolation changes only (Fig. 12, ORB-ONLY), whereas when forced with all relevant boundary conditions the correlation is still positive during the interglacial phases but negative in the glacial (Fig. 12, ALL). This change in correlation is due to the fact that SSTs decline into the glacial as a response to lower CO_2/ice-sheets but precipitation increases because of large-scale atmospheric circulation changes resulting from exposure of continental shelves in the Indo-Pacific (see section 4.3).

Over southern Africa, through the glacial cycle as a whole, there are generally negative correlations between SSTs and annual mean precipitation in the model, as the tropical rainbelt moves south as a global response to inter-hemispheric temperature gradients. Conversely, a positive correlation is found in response to Heinrich event simulations (induced by freshwater hosing the North Atlantic), as southern hemisphere SSTs warm and the rainbelt coincidently moves south, again in response to inter-hemispheric temperature gradients (Singarayer and Valdes, in review). In other words, a positive correlation results when southern SST changes echo changes in the overall temperature gradient.

Several of the relevant palaeorecords from SE Africa indicating positive correlations between SSTs and precipitation rely on pollen-based reconstructions (Truc et al., 2013; Dupont et al., 2011) and may approximate wet/growing season conditions rather than the annual mean (Truc et al., 2013). In HadCM3, LGM forcing results in southern hemisphere summer drying in this local area (Fig. S5), in contrast to the annual mean southern African response as a whole. The SSTs off the SW coast also cool producing a positive correlation between SSTs and austral summer precipitation. Here, this is the result of the ITCZ moving south and modifying the southern hemisphere Hadley circulation in austral summer to produce increased subsidence in the southern hemisphere subtropical high region, giving drier conditions off the coast of SE Africa specifically.

These examples illustrate that the correlations between SSTs and rainfall are temporally and spatially variable, depending on the primary driver of change and the interaction between different drivers. There is not always a causal relationship producing the correlations in the model. Consequently, it is not necessarily appropriate to extrapolate correlations seen in one region or over a particular time period to make more general hemispheric wide estimates of rainfall variation based on palaeo-SST records.

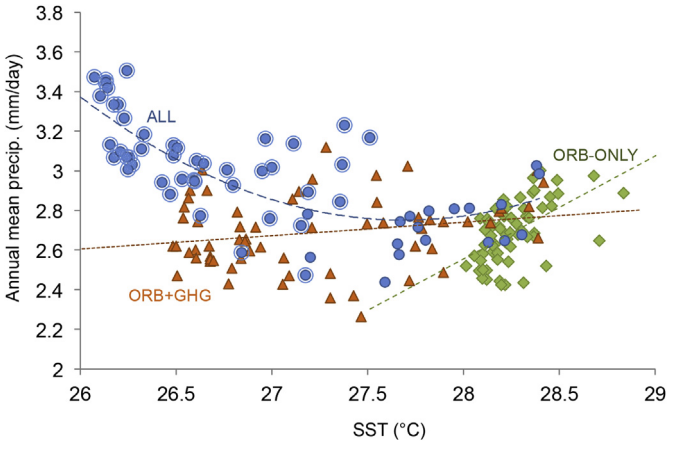

Fig. 12. Land-only mean annual precipitation vs. sea surface temperatures in the East African region (30–60°E, 10°S–0°S average) from the ORB-ONLY (green), ORB-GHG (orange), and ALL (blue) experiments in HadCM3. The circled blue points correspond to glacial time slices between 100 and 12 kyr BP for the ALL experiment where there are significant reductions in global sea level due to continental ice-sheet expansion. (For interpretation of the references to colour in this figure legend, the reader is referred to the web version of this article.)

5. Discussion

There is generally reasonable agreement between the collated palaeo-hydroclimate data and the HadCM3 suite of simulations covering the last glacial cycle. The model experiments suggest that the prevailing hypotheses (outlined in Section 2) for the modes of variation in wet-dry phases, which have at times been viewed in opposition, are not mutually exclusive. Different regions have differing sensitivities to driving mechanisms and, furthermore, the same mechanisms can influence equatorial regions differently than tropical regions to the north and south. For example, we find that HadCM3 (as well as most other PMIP3 models) undergoes a latitudinal shift north in the seasonal range of the rainbelt in the mid-Holocene, as found by calculating the change in the seasonal north/south latitudinal limits (section 4.1; Fig. 3b). However, apparent latitudinally symmetric wet-dry phases around West African equatorial regions are also a consequence of rainbelt variations (advected from the Atlantic) in HadCM3 (section 4.2).

In addition the primary mechanisms forcing changes in rainfall vary temporally as well as spatially. For example, in HadCM3 the equatorial east coast of Africa has a rainfall signature driven to a large extent by remote sea level changes in the Indo-Pacific during glacial periods (DiNezio and Tierney, 2013), but when ice volume is low (and sea level changes from PI are small) the contribution from local insolation changes in seasonality to rainfall variability are strong. These complications result in variability in the spatial patterns as well as temporal correlations. It is also the case that the amplitude of insolation forcing at the precessional time-scale has been relatively small over the last 50 kyr as we approach a 400-kyr minimum in eccentricity (Fig. S1). This may lead to increased prominence of other forcings (e.g. millennial-scale events) over this time period (Kuechler et al., 2013; Tjallingii et al., 2008). In HadCM3, during the latter half of the glacial cycle there is also a greater level of rainfall variability than during the first, due to internal coupled dynamics; this is particularly evident over southern Africa. Similar changes to wet-dry regimes have been observed in palaeorecords (e.g. Kuechler et al., 2013), but the paucity of long terrestrial palaeorainfall data means it is still difficult to robustly test the model outputs against the palaeo-record. Likewise, there are missing forcings and feedbacks (e.g. Dansgaard-Oschger events) in the model framework that currently inhibit progress.

In modern-day simulations, the African tropical rainbelt has smaller inter-model differences than other regions (Suzuki et al., 2011), leading to the suggestion that the seasonal march of the African rainbelt is relatively robust against differences in model physics and resolution. Indeed there are also regions where the mid-Holocene and LGM anomalies in tropical rainbelt precipitation are for the most part consistent between models. Northern Africa and the rainbelt north/south seasonal limits are regions where

there is the greatest agreement between models, e.g. northward expansion of the rainbelt into the Sahara during the mid-Holocene, which all models replicate (section 4.1), although they still generally underestimate the magnitude of the increase in rainfall (Braconnot et al., 2012; Pérez-Sanz et al., 2014). The modelling community has focussed significant effort into simulating and understanding past West African monsoon and northern African ITCZ changes (e.g. Marzin and Braconnot et al., 2007; Claussen and Gayler, 1997; Patricola and Cook, 2007). Much less attention has been paid to equatorial and southern hemisphere regions, partly because the signals from the palaeodata are not as clear as for northern Africa. In these regions the inter-model differences in hydroclimate changes during the mid-Holocene and LGM are significant, even though there is relative consistency in simulations of the present day. For example, models do not agree on the sign of MH-PI precipitation anomalies over equatorial West Africa (see section 4.2). Long terrestrial palaeodata records also become sparser towards the southern hemisphere, but if well synthesised, could provide valuable key targets for evaluation of future Earth system models.

Previous research by the authors and others has demonstrated the importance and complexity of the climate system response to the varying size of African surface waters (e.g. (Burrough et al., 2009b; Coe and Bonan, 1997; Contoux et al., 2013; Lauwaet et al., 2012) and changing vegetation assemblages (Brostrom et al., 1998; Claussen, 2009). Greatly expanded lake systems such as Mega-Lake Chad (MLC), which may have covered a surface area of up to 350,000 km^2 in the mid-Holocene (Leblanc et al., 2006; Schuster et al., 2005), have been found to have had a significant impact on modelled North African hydroclimate. The presence of MLC has feedbacks on rainfall that are negative at the local scale and positive at a larger scale. The lake inhibits deep convection processes due to its cold surface water (Krinner et al., 2012; Sepulchre et al., 2009) but doubles simulated precipitation rates in the central and western Sahara (Krinner et al., 2012), altering simulated climate variables at a comparable scale to changes due to orbital forcing alone (Coe and Bonan, 1997). Similarly in southern Africa, HadCM3 simulations run in conjunction with terrestrial biosphere models have demonstrated that the presence of large lake systems in the Late Quaternary such as mega-lake Makgadikgadi may not only have significantly amplified the seasonal distribution of rainfall in central southern Africa but potentially impacted both the composition and productivity of regional vegetation by up to 50% (Burrough et al., 2009). The impact of these large lake systems complicate predicted patterns of terrestrial hydroclimate response to orbital forcing alone, not only because they induce indirect feedback effects on climate and vegetation, but because variability in the lake surface area may be driven by precipitation changes in distant catchments. Lake response therefore, may not reflect localised precipitation changes (Burrough and Thomas, 2013; Burrough et al., 2009b). The inclusion of both lake/wetland and vegetation feedbacks in future model runs may help to better resolve and understand both the magnitude and spatial heterogeneity of hydroclimate change in Africa.

Palaeoproxy data provides a critical test of the model simulations discussed here, and our only window on to past climate change. The lens with which we can 'see' these changes however, is rarely free from distortion. The accuracy and resolution of chronological models that underpin the palaeoproxy time series are variable and will inevitably add an unknown and temporally varying degree of offset between records. The sensors that provide the proxy data also hold bias in the mechanisms through which they record changing rainfall. For example, hydrogen isotopes from the leaf waxes of past vegetation have been used extensively (both in this study and more widely) to make inferences about past rainfall amount/intensity but are also affected by 2nd order controls including relative humidity, the type of vegetation from which the leaf waxes are derived (Sachse et al., 2012), the seasonal timing of leaf-wax formation (Collins et al., 2014; Tipple et al., 2013), and the relative contribution of different rainfall source regions to the moisture that the plant incorporates into its molecular structure. All of these factors can change over time and may introduce systematic biases into the proxy records of past rainfall that make it challenging to unpick the precise nature of hydroclimate change and to differentiate changes in seasonality or circulation systems from total rainfall amount. In addition, the way in which these climate sensors become part of a palaeoclimate archive may also change over time with altering landscapes and depositional pathways so that for any one lake basin or ocean core, the size, shape and nature of the proxy source region may change over time. These issues of bias and distortion are not unique to δD and extend more generically to all proxy records discussed in this paper and may account for some degree of disagreement between different palaeo-rainfall records and between proxy data and model outputs. In future experiments, climate models that can simulate not only rainfall response but the predicted impact of these changes on the proxy record (e.g. the isotope-enabled models such as used by the NASA Goddard Institute for Space Studies (GISS) Model E-R (e.g. Tierney et al., 2011a) may facilitate much more robust model-data comparisons.

Additionally, palaeo-reconstructions of hydroclimate based on vegetation composition (derived from pollen records or $\delta^{13}C$ of vegetation) are likely to be influenced not just by changes in rainfall but also temperature and CO_2 (Harrison and Prentice, 2003). The effect of glacial CO_2 declines on plant competition in parallel with temperature and precipitation variations is extremely difficult to ascertain. Correction for the impact of CO_2 on palaeovegetation data is problematic without some method of process-based modelling (Khon et al., 2014). Offline simulations with the Biome4 model (Kaplan et al., 2003) driven with the HadCM3 glacial cycle simulations and different levels of CO_2 illustrate the potential for a large impact of CO_2 over the continent in the distribution of biomes (Fig. S8). Not being able to quantitatively correct for this in palaeovegetation-data-inferred rainfall changes may lead to overestimation of the magnitude of rainfall variability, produce patterns of temporal variability in inferred rainfall overly resembling CO_2 glacial-interglacial patterns (rather than precessional-scale variability), and/or produce artefacts in the inferred latitudinal patterns of change (Fig. S8c and d). In this study, we aimed to minimise this complicating factor by collating hydroclimate proxies that are not based on vegetation composition.

6. Conclusions

1. Many of the palaeo-data-driven hypotheses examined in this study through climate-model simulations were found to be at least partially valid, but the model outputs highlighted the sometimes neglected reality that at any one site, changes in rainfall could be associated with multiple forcing mechanisms and that the dominance of these forcing factors changed over time (also recently discussed by Otto-Bliesner et al., 2014, for the deglaciation). We find that palaeo-data driven hypotheses (e.g. meridonal vs zonal, interhemispheric asymmetry vs symmetrical changes to the rainbelt) are not mutually exclusive. This finding allows the community to move towards a more nuanced discussion of the driving mechanisms of tropical rainfall variation.
2. The relative lack of homogeneity in regional patterns of hydroclimate change in southern Africa when compared to northern

Africa is verified in both HadCM3 model experiments and in multi-model ensemble simulations for specific time periods including the mid-Holocene. The observed spatial heterogeneity is due to a more complex climate system than northern Africa, driven by the lower level of continentality and the greater role of oceanic influence on the tropical rainbelt.

3. The model experiments suggest that asymmetric movement in the tropical rainbelt occurs over Africa as a consequence of variations in insolation seasonality and continental-scale ice-sheet expansion/contraction. This asymmetry is of the latitudinal range of seasonal movement rather than reflecting movement in any particular season/month. As such, records towards the northern and southern seasonal limits are likely to demonstrate this asymmetry most readily. Records closer to the equator display more complex seasonality in rainfall (e.g. double rainfall peaks in the annual cycle). The response to local orbital insolation changes result in peak rainfall at times other than when the rainbelt is at its extreme north/south limits. In addition, other complicating factors play an important role in determining continental rainfall patterns (e.g. the influence of remote sea level changes on atmospheric circulation over East Africa).
4. There is a strong need for long terrestrial palaeorainfall records, particularly in Southern Africa where, as found in this study, the spatial heterogeneity of past rainfall changes is likely to be greater than in the Northern Hemisphere. Ocean cores, whilst providing valuable long, continuous records, integrate sediments derived from a broad area of the continental landmass, the boundaries of which remain fuzzy or unclear. Testing the mechanisms of hydroclimate change across the continent often remains limited to the Holocene by the number, short length and/or resolution of palaeorecords. There has been great progress made over the last two decades in increasing the number of long continental records (Brigham-Grette and Haug, 2007), particularly over East Africa. Ideally, a greater number of long terrestrial records are required, that capture periods of both high and low amplitude orbital precession and cover broader longitudinal and latitudinal transects across the continent, where possible, to more fully examine the behaviour of the tropical rainbelt and its relationship to orbital forcing.
5. The PMIP3 models demonstrate high levels of agreement over northern Africa, and lowest agreement towards coastal and equatorial regions. The markedly different responses in these regions primarily result from differing atmospheric physics parameterizations (e.g. convection) and differing land-atmosphere and/or ocean-atmosphere coupling strengths. As the modelling community potentially moves towards incorporating palaeoclimate within model development and tuning frameworks, spatially-resolved palaeodata syntheses of rainfall-related proxies from these terrestrial regions (see point 4) in particular would provide valuable targets for differentiating between model versions, and for improving process-based understanding of tropical hydroclimate variations.

Acknowledgements

JSS would like to thank Paul Valdes for collaboration on the initial HadCM3 glacial cycle suite of simulations, and acknowledges funding for this from the British Broadcasting Association (BBC). SLB would like to acknowledge funding by the Trapnell Fellowship and a National Geographic Global Exploration Award. JSS and SLB thank Richard Bailey for comments on the draft manuscript, and two anonymous reviewers who provided helpful and detailed comments.

Appendix A. Supplementary data

Supplementary data related to this article can be found at http://dx.doi.org/10.1016/j.quascirev.2015.06.021.

References

Bao, Q., Lin, P., Zhou, T., Liu, Y., Yu, Y., Wu, G., et al., 2013. The flexible global ocean-atmosphere-land system model, spectral version 2: FGOALS-s2. Adv. Atmos. Sci. 30, 561–576.
Bard, E., Rostek, F., Sonzogni, C., 1997. Interhemispheric synchrony of the last deglaciation inferred from alkenone palaeothermometry. Nature 707–710.
Barker, P., Williamson, D., Gasse, F., Gibert, E., 2003. Climatic and volcanic forcing revealed in a 50,000-year diatom record from Lake Massoko, Tanzania. Quat. Res. 60, 368–376.
Barker, P., Gasse, F., 2003. New evidence for a reduced water balance in East Africa during the Last Glacial Maximum: implication for model-data comparison. Quat. Sci. Rev. 22, 823–837.
Barker, P.A., Leng, M.J., Gasse, F., et al., 2007. Century-to-millennial scale climatic variability in Lake Malawi revealed by isotope records. Earth Planet. Sci. Lett. 261, 93–103.
Barker, P.A., Hurrell, E.R., Leng, M.J., Wolff, C., Cocquyt, C., Sloane, H.J., Verschuren, D., 2011. Seasonality in equatorial climate over the past 25 k.y. Revealed by oxygen isotope records from Kilimanjaro. Geology 39, 1111–1114.
Bartlein, P.J., Harrison, S.P., Brewer, S., Connor, S., Davis, B.A.S., Gajewski, K., Guiot, J., Harrison-Prentice, T.I., Hender- son, A., Peyron, O., Prentice, I.C., Scholze, M., Seppä, H., Shu- man, B., Sugita, S., Thompson, R.S., Viau, A.E., Williams, J., Wu, H., 2011. Pollen-based continental climate reconstructions at 6 and 21 ka: a global synthesis. Clim. Dynam. 37, 775–802. http://dx.doi.org/10.1007/s00382-010-0904-1.
Berger, A.L., 1978. Long-term variations of daily insolation and Quaternary climatic changes. J. Atmos. Sci. 2361–2367.
Berger, A., Loutre, M.F., 1991. Insolation values for the climate of the last 10 million years. Quat. Sci. Rev. 10, 297–317.
Berke, M.A., Johnson, T.C., Werne, J.P., Grice, K., Schouten, S., Sinninghe Damsté, J.S., 2012. Molecular records of climate variability and vegetation response since the Late Pleistocene in the Lake Victoria basin, East Africa. Quat. Sci. Rev. 55, 59–74.
Braconnot, P., Otto-Bliesner, B., Harrison, S., Joussaume, S., Peterchmitt, J.-Y., Abe-Ouchi, A., Crucifix, M., Driesschaert, E., Fichefet, Th, Hewitt, C.D., Kageyama, M., Kitoh, A., Loutre, M.-F., Marti, O., Merkel, U., Ramstein, G., Valdes, P., Weber, L., Yu, Y., Zhao, Y., 2007. Results of PMIP2 coupled simulations of the Mid-Holocene and Last Glacial Maximum – Part 2: feedbacks with emphasis on the location of the ITCZ and mid- and high latitudes heat budget. Clim. Past. 3, 279–296.
Braconnot, P., Harrison, S.P., Kageyama, M., Bartlein, P.J., Masson-Delmotte, V., Abe-Ouchi, A., Otto-Bliesner, B., Zhao, Y., 2012. Evaluation of climate models using palaeoclimatic data. Nature Climate Change 2, 417–424.
Brigham-Grette, J., Haug, G., 2007. Climate dynamics and global environments: a community vision for the next decade in ICDP. In: Harms, U., Koeberl, C., Zoback, M.D. (Eds.), Continental Scientific Drilling: a Decade of Progress and Challenges for the Future. Spinrger Berlin Heidelberg, New York, pp. 53–94.
Broccoli, A.J., Dahl, K.A., Stouffer, R.J., 2006. Response of the ITCZ to Northern Hemisphere cooling. Geophys. Res. Lett. 33 (1).
Brostrom, A., Coe, M., Harrison, S.P., Gallimore, R., Kutzbach, J.E., Foley, J., Prentice, I.C., Behling, P., 1998. Land surface feedbacks and palaeomonsoons in northern Africa. Geophys. Res. Lett. 25, 3615–3618.
Brovkin, V., Claussen, M., 2008. Comment on "climate-driven ecosystem succession in the Sahara: the past 6000 years". Science 322.
Burnett, A.P., Soreghan, M.J., Scholz, C.A., Brown, E.T., 2011. Tropical East African climate change and its relation to global climate: a record from Lake Tanganyika, Tropical East Africa, over the past 90+kyr. Palaeogeogr. Palaeoclimatol. Palaeoecol. 303, 155–167.
Burrough, S.L., Thomas, D.S.G., 2013. Central southern Africa at the time of the African Humid Period: a new analysis of Holocene palaeoenvironmental and palaeoclimate data. Quat. Sci. Rev. 80, 29–46.
Burrough, S.L., Thomas, D.S.G., Bailey, R.M., 2009a. Mega-Lake in the Kalahari: a late Pleistocene record of the Palaeolake Makgadikgadi system. Quat. Sci. Rev. 28, 1392–1411.
Burrough, S.L., Thomas, D.S.G., Singarayer, J.S., 2009b. Late Quaternary hydrological dynamics in the Middle Kalahari: forcing and feedbacks. Earth Sci. Rev. 96, 313–326.
Castañeda, I.S., Werne, J.P., Johnson, T.C., 2007. Wet and arid phases in the southeast African tropics since the Last Glacial Maximum. Geology 35, 823–826.
Cattle, H., Crossley, J., 1995. Modelling Arctic climate-change. Philos. Trans. R. Soc. A 352, 201–213.
Chase, B.M., Meadows, M.E., 2007. Late Quaternary dynamics of southern Africa's winter rainfall zone. Earth Sci. Rev. 103–138.
Chase, B.M., Meadows, M.E., Carr, A.S., Reimer, P.J., 2010. Evidence for progressive holocene aridification in southern Africa recorded in Namibian hyrax middens: implications for African Monsoon dynamics and the 'African Humid Period'. Quat. Res. 74, 36–45.

Chase, B.M., Meadows, M.E., Scott, L., Thomas, D.S.G., Marais, E., Sealy, J., Reimer, P.J., 2009. A record of rapid Holocene climate change preserved in hyrax middens from southwestern Africa. Geology 37, 703–706.
Chiang, J.C., Bitz, C.M., 2005. Influence of high latitude ice cover on the marine Intertropical Convergence Zone. Clim. Dyn. 25 (5), 477–496.
Claussen, M., 2009. Late Quaternary vegetation-climate feedbacks. Clim. Past 5, 203–216.
Claussen, M., Gayler, V., 1997. The greening of the Sahara during the mid-Holocene: results of an interactive atmosphere-biome model. Glob. Ecol. Biogeogr. Lett. 369–377.
Claussen, M., Bathiany, S., Brovkin, V., Kleinen, T., 2013. Simulated climate-vegetation interaction in semi-arid regions affected by plant diversity. Nat. Geosci. 6 (11), 954–958.
Cockcroft, M.J., Wilkinson, M.J., Tyson, P.D., 1987. The application of a present-day climatic model to the late Quaternary in southern Africa. Clim. Change 161–181.
Coe, M.T., Bonan, G.B., 1997. Feedbacks between climate and surface water in northern Africa during the middle Holocene. J. Geophys. Res. D: Atmos. 102, 11087–11101.
Cohen, A.S., Stone, J.R., Beuning, K.R.M., Park, L.E., Reinthal, P.N., Dettman, D., Scholz, C.A., Johnson, T.C., King, J.W., Talbot, M.R., Brown, E.T., Ivory, S.J., 2007. Ecological consequences of early Late Pleistocene megadroughts in tropical Africa. Proc. Natl. Acad. Sci. USA 104, 16422–16427.
Collins, J.A., Schefuß, E., Govin, A., Mulitza, S., Tiedemann, R., 2014. Insolation and glacial-interglacial control on southwestern African hydroclimate over the past 140000 years. Earth Planet. Sci. Lett. 398, 1–10.
Collins, J.A., Schefuß, E., Heslop, D., Mulitza, S., Prange, M., Zabel, M., Tjallingii, R., Dokken, T.M., Huang, E., MacKensen, A., Schulz, M., Tian, J., Zarriess, M., Wefer, G., 2011a. Interhemispheric symmetry of the tropical African rainbelt over the past 23,000 years. Nat. Geosci. 4, 42–45.
Contoux, C., Jost, A., Ramstein, G., Sepulchre, P., Krinner, G., Schuster, M., 2013. Megalake chad impact on climate and vegetation during the late Pliocene and the mid-Holocene. Clim. Past 9, 1417–1430.
Collins, W.J., Bellouin, N., Doutriaux-Boucher, M., Gedney, N., Halloran, P., Hinton, T., Hughes, J., Jones, C.D., Joshi, M., Lid- dicoat, S., Martin, G., O'Connor, F., Rae, J., Senior, C., Sitch, S., Totterdell, I., Wiltshire, A., Woodward, S., 2011b. Development and evaluation of an Earth-System model – HadGEM2. Geosci. Model Dev. 4, 1051–1075. http://dx.doi.org/10.5194/gmd-4-1051-2011.
Costa, K., Russell, J., Konecky, B., Lamb, H., 2014. Isotopic reconstruction of the African Humid Period and Congo Air Boundary migration at Lake Tana, Ethiopia. Quat. Sci. Rev. 83, 58–67.
Cox, P.M., 2001. Description of the TRIFFID Dynamic Global Vegetation Model. Technical Note 24. Hadley Centre.
Dee, D.P., Uppala, S.M., Simmons, A.J., Berrisford, P., Poli, P., Kobayashi, S., Andrae, U., Balmaseda, M.A., Balsamo, G., Bauer, P., Bechtold, P., Beljaars, A.C.M., van de Berg, L., Bidlot, J., Bormann, N., Delsol, C., Dragani, R., Fuentes, M., Geer, A.J., Haimberger, L., Healy, S.B., Hersbach, H., Hólm, E.V., Isaksen, L., Kållberg, P., Köhler, M., Matricardi, M., McNally, A.P., Monge-Sanz, B.M., Morcrette, J.-J., Park, B.-K., Peubey, C., de Rosnay, P., Tavolato, C., Thépaut, J.-N., Vitart, F., 2011. The ERA-Interim reanalysis: configuration and performance of the data assimilation system. Q.J.R. Meteorol. Soc. 137, 553–597. http://dx.doi.org/10.1002/qj.828.
DeMenocal, P., Ortiz, J., Guilderson, T., Sarnthein, M., 2000. Coherent high- and low-latitude climate variability during the Holocene warm period. Science 2198–2202.
Demenocal, P.B., Ruddiman, W.F., Pokras, E.M., 1993. Influence of high- and low-latitude processes on African terrestrial climate: Pleistocene eolian records from equatorial Atlantic Ocean Drilling Program Site 663. Paleoceanography 8, 209–242.
DiNezio, P.N., Tierney, J.E., 2013. The effect of sea level on glacial Indo-Pacific climate. Nat. Geosci. 6 (6), 485–491.
Dufresne, J.-L., Foujols, M.-A., Denvil, S., Caubel, A., Marti, O., Aumont, O., Balkanski, Y., Bekki, S., Bellenger, H., Ben- shila, R., 2013. Climate change projections using the IPSL-CM5 Earth System Model: from CMIP3 to CMIP5. Clim. Dynam. 9–10, 2123–2165. http://dx.doi.org/10.1007/s00382-012-1636-1.
Dupont, L.M., Caley, T., Kim, J.H., Castañeda, I., Malaizé, B., Giraudeau, J., 2011. Glacial-interglacial vegetation dynamics in South Eastern Africa coupled to sea surface temperature variations in the Western Indian Ocean. Clim. Past 7, 1209–1224.
Edwards, J.M., Slingo, A., 1996. Studies with a flexible new radiation code.1. Choosing a configuration for a large-scale model. Q.J. R. Met. Soc. 122, 689–719.
Eriksson, A., Betti, L., Friend, A.D., Lycett, S.J., Singarayer, J.S., von Cramon-Taubadel, N., Manica, A., 2012. Late Pleistocene climate change and the global expansion of anatomically modern humans. Proc. Natl. Acad. Sci. 109 (40), 16089–16094.
Essery, R., Best, M., Cox, P., 2001. MOSES 2.2 Technical Documentation. Technical Note 30. Hadley Centre.
Finney, B.P., Sholz, C.A., Johnson, T.C., et al., 1996. Late Quaternary Lake-level Changes of Lake Malawi. In: The Limnology, Climatology and Paleoclimatology of the East African Lakes, pp. 495–508.
Gasse, F., Barker, P., Johnson, T., 2002. A 24,000 yr Diatom Record from the Northern Basin of Lake Malawi. In: Odada, E., Olago, D. (Eds.), The East African Great Lakes: Limnology, Palaeolimnology and Biodiversity, pp. 393–414. Springer Netherlands.
Gasse, F., Chalie, F., Vincens, A., Williams, M.A.J., Williamson, D., 2008. Climatic patterns in equatorial and southern Africa from 30,000 to 10,000 years ago reconstructed from terrestrial and near-shore proxy data. Quat. Sci. Rev. 27, 2316–2340.
Garcin, Y., Vincens, A., Williamson, D., Guiot, J., Buchet, G., 2006. Wet phases in tropical southern Africa during the last glacial period. Geophys. Res. Lett. 33.
Garcin, Y., Junginger, A., Melnick, D., Olago, D.O., Strecker, M.R., Trauth, M.H., 2009. Late Pleistocene-Holocene rise and collapse of Lake Suguta, northern Kenya rift. Quat. Sci. Rev. 28, 911–925.
Gent, P.R., McWilliams, J.C., 1990. Isopycnal mixing in ocean circulation models. J. Phys. Oceanogr. 20, 150–155.
Gent, P.R., Danabasoglu, G., Donner, L.J., Holland, M.M., Hunke, E.C., Jayne, S.R., Lawrence, D.M., Neale, R.B., Rasch, P.J., Vertenstein, M., 2011. The community climate system model version 4. J. Clim. 24, 4973–4991. http://dx.doi.org/10.1175/2011JCLI4083.1.
Gordon, C., Cooper, C., Senior, C.A., Banks, H., Gregory, J.M., Johns, T.C., Mitchell, J.F.B., Wood, R.A., 2000. The simulation of SST, sea ice extents and ocean heat transports in a version of the Hadley Centre coupled model without flux adjustments. Clim. Dyn. 16, 147–168.
Govin, A., Varma, V., Prange, M., 2014. Astronomically forced variations in western African rainfall (21°N–20°S) during the Last Interglacial period. Geophys. Res. Lett. 41, 2117–2125.
Heine, K., 1982. The main stages of the late Quaternary evolution of the Kalahari region, southern Africa. Palaeoecol. Afr. 15, 53–76.
Harrison, S.P., Prentice, C.I., 2003. Climate and CO_2 controls on global vegetation distribution at the last glacial maximum: analysis based on palaeovegetation data, biome modelling and palaeoclimate simulations. Glob. Change Biol. 9, 983–1004.
Holton, J.R., Wallace, J.M., Young, J.A., 1971. On boundary layer dynamics and the ITCZ. J. Atmos. Sci. 28, 275–280.
Huang, J., Wang, S., Wen, X., Yang, B., 2008. Progress in studies of the climate of humid period and the impacts of changing precession in early-mid Holocene. Prog. Nat. Sci. 18, 1459–1464.
Johnson, T.C., 1996. Sedimentary Processes and Signals of Past Climatic Change in the Large Lakes of the East African Rift Valley. In: The Limnology, Climatology and Paleoclimatology of the East African Lakes, pp. 367–412.
Johnson, T.C., 2002. Biogenic Silica Profiles in the Sediments of Large Tropical Lakes: Examples from East Africa. In: Sedimentation in Continental Rifts, pp. 247–255.
Jungclaus, J.H., Keenlyside, N., Botzet, M., Haak, H., Luo, J.J., Latif, M., Marotzke, J., Mikolajewicz, U., Roeckner, E., 2006. Ocean circulation and tropical variability in the coupled model ECHAM5/MPI-OM. J. Clim. 19, 3952–3972.
Jury, M.R., Valentine, H.R., Lutjeharms, J.R.E., 1993. Influence of the Agulhas Current on summer rainfall along the southeast coast of South Africa. J. Appl. Meteorol. 32, 1282–1287.
Kaplan, J.O., Bigelow, N.H., Bartlein, P.J., Christensen, T.R., Cramer, W., Harrison, S.P., Matveyeva, N.V., McGuire, A.D., Murray, D.F., Prentice, I.C., Razzhivin, V.Y., Smith, B., Walker, D.A., Anderson, P.M., Andreev, A.A., Brubaker, L.B., Edwards, M.E., Lozhkin, A.V., Ritchie, J., 2003. Climate change and Arctic ecosystems II: Modeling, palaeodata-model comparisons, and future projections. J. Geophys. Res. Atmos. 108 (D19), 8171.
Khon, V.C., Wang, Y.V., Krebs-Kanzow, U., Kaplan, J.O., Schneider, R.R., Schneider, B., 2014. Climate and CO_2 effects on the vegetation of southern tropical Africa over the last 37,000 years. Earth Planet. Sci. Lett. 403, 407–417.
Konecky, B.L., Russell, J.M., Johnson, T.C., Brown, E.T., Berke, M.A., Werne, J.P., Huang, Y., 2011. Atmospheric circulation patterns during late Pleistocene climate changes at Lake Malawi, Africa. Earth Planet. Sci. Lett. 312, 318–326.
Krinner, G., Lézine, A.M., Braconnot, P., Sepulchre, P., Ramstein, G., Grenier, C., Gouttevin, I., 2012. A reassessment of lake and wetland feedbacks on the North African Holocene climate. Geophys. Res. Lett. 39.
Kröpelin, S., Verschuren, D., Lézine, A.M., Eggermont, H., Cocquyt, C., Francus, P., Cazet, J.P., Fagot, M., Rumes, B., Russell, J.M., Darius, F., Conley, D.J., Schuster, M., Von Suchodoletz, H., Engstrom, D.R., 2008. Climate-driven ecosystem succession in the Sahara: the past 6000 years. Science 320, 765–768.
Kuechler, R.R., Schefuß, E., Beckmann, B., Dupont, L., Wefer, G., 2013. NW African hydrology and vegetation during the Last Glacial cycle reflected in plant-wax-specific hydrogen and carbon isotopes. Quat. Sci. Rev. 82, 56–67.
Kutzbach, J.E., Liu, X., Liu, Z., Chen, G., 2008. Simulation of the evolutionary response of global summer monsoons to orbital forcing over the past 280,000 years. Clim. Dyn. 30, 567–579.
Kutzbach, J.E., Liu, Z., 1997. Response of the African monsoon to orbital forcing and ocean feedbacks in the middle Holocene. Science 278, 440–443.
Lauwaet, D., van Lipzig, N.P.M., Van Weverberg, K., De Ridder, K., Goyens, C., 2012. The precipitation response to the desiccation of Lake Chad. Q. J. R. Meteorol. Soc. 138, 707–719.
Leblanc, M., Favreau, G., Maley, J., Nazoumou, Y., Leduc, C., Stagnitti, F., van Oevelen, P.J., Delclaux, F., Lemoalle, J., 2006. Reconstruction of Megalake Chad using Shuttle Radar Topographic Mission data. Palaeogeogr. Palaeoclimatol. Palaeoecol. 239, 16–27.
Lézine, A.M., Hély, C., Grenier, C., Braconnot, P., Krinner, G., 2011. Sahara and Sahel vulnerability to climate changes, lessons from Holocene hydrological data. Quat. Sci. Rev. 30, 3001–3012.
Li, G., Harrison, S.P., Bartlein, P.J., Izumi, K., Colin Prentice, I., 2013. Precipitation scaling with temperature in warm and cold climates: an analysis of CMIP5 simulations. Geophys. Res. Lett. 40, 4018–4024. http://dx.doi.org/10.1002/grl.50730.

Liu, Z., Otto-Bliesner, B., Kutzbach, J., Li, L., Shields, C., 2003. Coupled climate simulation of the evolution of global monsoons in the Holocene. J. Clim. 16, 2472–2490.
Loulergue, L., Schilt, A., Spahni, R., Masson-Delmotte, V., Blunier, T., Lemieux, B., Barnola, J.-M., Raynaud, D., Stocker, T.F., Chappellaz, J., 2008. Orbital and millennial-scale features of atmospheric CH4 over the past 800,000years. Nature 453, 383–386.
Marzin, C., Braconnot, P., 2009. Variations of Indian and African monsoons induced by insolation changes at 6 and 9.5 kyr BP. Clim. Dyn. 33 (2–3), 215–231.
Moernaut, J., Verschuren, D., Charlet, F., Kristen, I., Fagot, M., De Batist, M., 2010. The seismic-stratigraphic record of lake-level fluctuations in Lake Challa: hydrological stability and change in equatorial East Africa over the last 140 kyr. Earth Planet. Sci. Lett. 290, 214–223.
Nicholson, S., 2009. A revised picture of the structure of the “monsoon” and land ITCZ over West Africa. Clim. Dyn. 32, 1155–1171.
Niedermeyer, E.M., Schefuß, E., Sessions, A.L., Mulitza, S., Mollenhauer, G., Schulz, M., Wefer, G., 2010. Orbital- and millennial-scale changes in the hydrologic cycle and vegetation in the western African Sahel: insights from individual plant wax δD and δ13C. Quat. Sci. Rev. 29, 2996–3005.
Otto-Bliesner, B.L., Russell, J.M., Clark, P.U., Liu, Z., Overpeck, J.T., Konecky, B., Nicholson, S.E., He, F., Lu, Z., 2014. Coherent changes of southeastern equatorial and northern African rainfall during the last deglaciation. Science 346, 1223–1227.
Parrenin, F., Barnola, J.-M., Beer, J., Blunier, T., Castellano, E., Chappellaz, J., Dreyfus, G., Fischer, H., Fujita, S., Jouzel, J., Kawamura, K., Lemieux-Dudon, B., Loulergue, L., Masson-Delmotte, V., Narcisi, B., Petit, J.-R., Raisbeck, G., Raynaud, D., Ruth, U., Schwander, J., Severi, M., Spahni, R., Steffensen, J.P., Svensson, A., Udisti, R., Waelbroeck, C., Wolff, E., 2007. The EDC3 agescale for the EPICA dome C ice core. Clim. Past. 3, 485–497.
Partridge, T.C., deMenocal, P.B., Lorentz, S.A., Paiker, M.J., Vogel, J.C., 1997a. Orbital forcing of climate over South Africa: a 200,000-year rainfall record from the Pretoria Saltpan. Quat. Sci. Rev. 16, 1125–1133.
Partridge, T.C., Demenocal, P.B., Lorentz, S.A., Paiker, M.J., Vogel, J.C., 1997b. Orbital forcing of climate over South Africa: a 200,000-year rainfall record from the Pretoria Saltpan. Quat. Sci. Rev. 1125–1133.
Patricola, C.M., Cook, K.H., 2007. Dynamics of the West African monsoon under mid-Holocene precessional forcing: regional climate model simulations. J. Clim. 20 (4), 694–716.
Peck, J.A., Green, R.R., Shanahan, T., King, J.W., Overpeck, J.T., Scholz, C.A., 2004. A magnetic mineral record of Late Quaternary tropical climate variability from Lake Bosumtwi, Ghana. Palaeogeogr. Palaeoclimatol. Palaeoecol. 215, 37–57.
Peltier, W.R., 2004. Global glacial isostasy and the surface of the iceage Earth: the ICE-5G (VM2) model and GRACE. Annu. Rev. Earth Planet Sci. 32, 111–149.
Pérez Sanz, A., Li, G., González Sampériz, P., Harrison, S.P., 2014. Evaluation of modern and mid-Holocene seasonal precipitation of the Mediterranean and northern Africa in the CMIP5 simulations. Clim. Past 10, 551–568.
Petit, J.R., Jouzel, J., Raynaud, D., Barkov, N.I., Barnola, J.-M., Basile, I., Bender, M., Chappellaz, J., Davis, J., Delaygue, G., Delmotte, M., Kotlyakov, V.M., Legrand, M., Lipenkov, V., Lorius, C., Pepin, L., Ritz, C., Saltzman, E., Stievenard, M., 1999. Climate and atmospheric history of the past 420000 years from the Vostok Ice Core, Antarctica. Nature 399, 429–436.
Pokras, E.M., Mix, A.C., 1987. Earth's precession cycle and Quaternary climatic change in tropical Africa. Nature 326, 486–487.
Pope, V.D., Gallani, M.L., Rowntree, P.R., Stratton, R.A., 2000. The impact of new physical parameterisations in the Hadley Centre climate model: HadAM3. Clim. Dyn. 16, 123–146.
Prell, W.L., Kutzbach, J.E., 1987. Monsoon variability over the past 150,000 years. J. Geophys. Res. 92, 8411–8425.
Reason, C.J.C., Mulenga, H., 1999. Relationships between South African rainfall and SST anomalies in the southwest Indian Ocean. Int. J. Climatol. 1651–1673.
Rossignol-Strick, M., 1983. African monsoons, an immediate climate response to orbital insolation. Nature 304, 46–49.
Rotstayn, L.D., Collier, M.A., Dix, M.R., Feng, Y., Gordon, H.B., O'Farrell, S.P., Smith, I.N., Syktus, J., 2010. Improved simulation of Australian climate and ENSO-related rainfall variability in a global climate model with an interactive aerosol treatment. Int. J. Climatol. 30, 1067–1088. http://dx.doi.org/10.1002/joc.1952.
Sachse, D., Billault, I., Bowen, G.J., Chikaraishi, Y., Dawson, T.E., Feakins, S.J., Freeman, K.H., Magill, C.R., McInerney, F.A., Van Der Meer, M.T.J., Polissar, P., Robins, R.J., Sachs, J.P., Schmidt, H.L., Sessions, A.L., White, J.W.C., West, J.B., Kahmen, A., 2012. Molecular paleohydrology: interpreting the hydrogen-isotopic composition of lipid biomarkers from photosynthesizing organisms. Annu. Rev. Earth Planet. Sci. 40, 221–249.
Schefuß, E., Kuhlmann, H., Mollenhauer, G., Prange, M., Pätzold, J., 2011. Forcing of wet phases in southeast Africa over the past 17,000 years. Nature 480, 509–512.
Schefuß, E., Schouten, S., Schneider, R.R., 2005. Climatic controls on central African hydrology during the past 20,000 years. Nature 437, 1003–1006.
Schmidt, G.A., Kelley, M., Nazarenko, L., Ruedy, R., Russell, G.L., Aleinov, I., Bauer, M., Bauer, S.E., Bhat, M.K., Bleck, R., Canuto, V., Chen, Y.-H., Cheng, Y., Clune, T.L., Del Genio, A., de Fainchtein, R., Faluvegi, G., Hansen, J.E., Healy, R.J., Kiang, N.Y., Koch, D., Lacis, A.A., LeGrande, A.N., Lerner, J., Lo, K.K., Matthews, E.E., Menon, S., Miller, R.L., Oinas, V., Oloso, A.O., Perlwitz, J.P., Puma, M.J., Putman, W.M., Rind, D., Ro- manou, A., Sato, M., Shindell, D.T., Sun, S., Syed, R.A., Taus- nev, N., Tsigaridis, K., Unger, N., Voulgarakis, A., Yao, M.-S., Zhang, J., 2014. Configuration and assessment of the GISS Mod-elE2 contributions to the CMIP5 archive. J. Adv. Model. Earth Syst. 6, 1–44. http://dx.doi.org/10.1002/2013MS000265.
Scholz, C.A., Johnson, T.C., Cohen, A.S., King, J.W., Peck, J.A., Overpeck, J.T., Talbot, M.R., Brown, E.T., Kallndekafe, L., Amoako, P.Y.O., Lyons, R.P., 2007. East African megadroughts between 135 and 75 thousand years ago and bearing on early-modern human origins. PNAS 104, 16416–16421.
Schuster, M., Roquin, C., Duringer, P., Brunet, M., Caugy, M., Fontugne, M., Mackaye, H.T., Vignaud, P., Ghienne, J.-F., 2005. Holocene Lake Mega-Chad palaeoshorelines from space. Quat. Sci. Rev. 24, 1821–1827.
Sepulchre, P., Ramstein, G., Schuster, M., 2009. Modelling the impact of tectonics, surface conditions and sea surface temperatures on Saharan and sub-Saharan climate evolution. Comptes Rendus - Geosci. 341, 612–620.
Shanahan, T.M., McKay, N.P., Hughen, K.A., Overpeck, J.T., Otto-Bliesner, B., Heil, C.W., Scholz, C.A., Peck, J., 2015. The time-transgressive termination of the African Humid Period. Nat. Geosci. 8, 140–144.
Shi, N., Schneider, R., Beug, H.-J., Dupont, L.M., 2001. Southeast trade wind variations during the last 135 kyr: evidence from pollen spectra in eastern South Atlantic sediments. Earth Planet. Sci. Lett. 187, 311–321.
Singarayer, J.S., Valdes, P.J., 2010. High-latitude climate sensitivity to ice-sheet forcing over the last 120kyr. Quat. Sci. Rev. 29 (1), 43–55.
Singarayer, J.S., Valdes, P.J., 2015. Latitudinal migration vs. expansion/contraction of the tropical rainbelt in the last 120kyr. Nat. Geosci. (submitted for publication).
Singarayer, J.S., Valdes, P.J., Friedlingstein, P., Nelson, S., Beerling, D.J., 2011. Late Holocene methane rise caused by orbitally controlled increase in tropical sources. Nature 470 (7332), 82–85.
Sonzogni, C., Bard, E., Rostek, F., 1998. Tropical sea-surface temperatures during the last glacial period: a view based on alkenones in Indian Ocean sediments. Quat. Sci. Rev. 17, 1185–1201.
Spahni, R., Chappellaz, J., Stocker, T.F., Loulergue, L., Hausammann, G., Kawamura, K., Fluckiger, J., Schwander, J., Raynaud, D., Masson-Delmotte, V., Jouzel, J., 2005. Variations of atmospheric methane and nitrous oxide during the last 650,000 years from Antarctic ice cores. Science 310, 1317–1321.
Stager, J.C., 1988. Environmental changes at Lake Cheshi, Zambia since 40,000years BP. Quartern. Res. 29, 54–65.
Stokes, S., Thomas, D.S.G., Washington, R., 1997. Multiple episodes of aridity in southern Africa since the last interglacial period. Nature 388, 154–158.
Street-Perrott, F.A., Marchand, D.S., Roberts, N., et al., 1989. Global Lake Level Variations from 18,000 to 0 Years Ago: a Palaeoclimatic Analysis. Department of Energy, Washington, p. 213.
Stuut, J.-B.W., Prins, M.A., Schneider, R.R., Weltje, G.J., Jansen, J.H.F., Postma, G., 2002a. A 300-kyr record of aridity and wind strength in southwestern Africa: Inferences from grain-size distributions of sediments on Walvis Ridge, SE Atlantic. Mar. Geol. 180, 221–233.
Stuut, J.-B.W., Prins, M.A., Schneider, R.R., Weltje, G.J., Jansen, J.H.F., Postma, G., 2002b. A 300 kyr record of aridity and wind strength in southwestern Africa: inferences from grain-size distributions of sediments on Walvis Ridge, SE Atlantic. Mar. Geol. 180, 221–233.
Stuut, J.B.W., Crosta, X., van der Borg, K., Schneider, R., 2004. Relationship between Antarctic sea ice and southwest African climate during the late Quaternary. Geology 32, 909–912.
Taylor, K.E., Stouffer, R.J., Meehl, G.A., 2012. An overview of CMIP5 and the experiment design. Bull. Am. Meteorol. Soc. 93, 485–498.
Thomas, D.S.G., Bailey, R., Shaw, P.A., Durcan, J.A., Singarayer, J.S., 2009. Late Quaternary highstands at Lake Chilwa, Malawi: frequency, timing and possible forcing mechanisms in the last 44 ka. Quat. Sci. Rev. 28, 526–539.
Tierney, J.E., DeMenocal, P.B., 2013. Abrupt shifts in Horn of Africa hydroclimate since the last glacial maximum. Science 342, 843–846.
Tierney, J.E., Lewis, S.C., Cook, B.I., LeGrande, A.N., Schmidt, G.A., 2011a. Model, proxy and isotopic perspectives on the East African Humid Period. Earth Planet. Sci. Lett. 307, 103–112.
Tierney, J.E., Russell, J.M., Huang, Y., 2010. A molecular perspective on Late Quaternary climate and vegetation change in the Lake Tanganyika basin, East Africa. Quat. Sci. Rev. 29, 787–800.
Tierney, J.E., Russell, J.M., Huang, Y., Sinninghe DamstÃ©, J.S., Hopmans, E.C., Cohen, A.S., 2008. Northern hemisphere controls on tropical southeast African climate during the past 60,000 years. Science 322, 252–255.
Tierney, J.E., Russell, J.M., Sinninghe Damsté, J.S., Huang, Y., Verschuren, D., 2011b. Late Quaternary behavior of the East African monsoon and the importance of the Congo Air Boundary. Quat. Sci. Rev. 30, 798–807.
Tipple, B.J., Berke, M.A., Doman, C.E., Khachaturyan, S., Ehleringer, J.R., 2013. Leaf-wax n-alkanes record the plant-water environment at leaf flush. Proc. Natl. Acad. Sci. USA 110, 2659–2664.
Tjallingii, R., Claussen, M., Stuut, J.B.W., Fohlmeister, J., Jahn, A., Bickert, T., Lamy, F., Röhl, U., 2008. Coherent high- and low-latitude control of the northwest African hydrological balance. Nat. Geosci. 1, 670–675.
Trauth, M.H., Deino, A.L., Bergner, A.G.N., Strecker, M.R., 2003. East Africam climate change and orbital forcing during the last 175 kyr BP. Earth Planet. Sci. Lett. 297–313.
Truc, L., Chevalier, M., Favier, C., Cheddadi, R., Meadows, M.E., Scott, L., Carr, A.S., Smith, G.F., Chase, B.M., 2013. Quantification of climate change for the last 20,000 years from Wonderkrater, South Africa: implications for the long-term dynamics of the Intertropical Convergence Zone. Palaeogeogr. Palaeoclimatol. Palaeoecol. 386, 575–587.

van Zinderen Bakker, E.M., 1976. The evolution of late Quaternary paleoclimates of Southern Africa. Palaeoecol. Afr. 9, 160–202.

Verschuren, D., Sinninghe Damsté, J.S., Moernaut, J., et al., 2009. Half-precessional dynamics of monsoon rainfall near the East African Equator. Nature 462, 637–641.

Vincens, A., Buchet, G., Williamson, D., Taieb, M., 2005. A 23,000 yr pollen record from Lake Rukwa (8*S, SW Tanzania): new data on vegetation dynamics and climate in Central Eastern Africa. Rev. Palaeobot. Palynol. 137, 147–162.

Voldoire, A., Sanchez-Gomez, E., y Mélia, D.S., Decharme, B., Cassou, C., Sénési, S., Valcke, S., Beau, I., Alias, A., Chevallier, M., 2013. The CNRM-CM5, 1 global climate model: description and basic evaluation. Clim. Dynam. 9–10, 2091–2121. http://dx.doi.org/10.1007/s00382-011-1259-y.

Watanabe, S., Hajima, T., Sudo, K., Nagashima, T., Takemura, T., Okajima, H., Nozawa, T., Kawase, H., Abe, M., Yokohata, T., Ise, T., Sato, H., Kato, E., Takata, K., Emori, S., Kawamiya, M., 2011. MIROC-ESM 2010, model description and basic results of CMIP5-20c3m experiments. Geosci. Model Dev. 4, 845–872. http://dx.doi.org/10.5194/gmd-4-845-2011.

Weldeab, S., Lea, D.W., Schneider, R.R., Andersen, N., 2007. 155,000 years of West African monsoon and ocean thermal evolution. Science 316, 1303–1307.

Wu, T., Li, W., Ji, J., Xin, X., Li, L., Wang, Z., Zhang, Y., Li, J., Zhang, F., Wei, M., 2013. Global carbon budgets simulated by the Beijing Climate Center Climate System Model for the last century. J. Geophys. Res. Atmos. 118, 4326–4347. http://dx.doi.org/10.1002/jgrd.50320.

Yukimoto, S., Yoshimura, H., Hosaka, M., Sakami, T., Tsujino, H., Hirabara, M., Tanaka, T.Y., Deushi, M., Obata, A., Nakano, H., Adachi, Y., Shindo, E., Yabu, S., Ose, T., Kitoh, A., 2011. Meteorological Research Institute Earth System Model Version 1 (MRI-ESM1): Model Description. Technical reports of the me. teorological research institute No. 64, Meteorological Research Institute, Japan, p. 88.

Interhemispheric dynamics of the African rainbelt during the late Quaternary

Joy S. Singarayer[a*] & Sallie L. Burrough[b]

a: Department of Meteorology and Centre for Past Climate Change, University of Reading, RG6 6BB

b: Environmental Change Institute, University of Oxford, OX1 3QY

** Corresponding author: j.s.singarayer@reading.ac.uk*

Supplementary Information

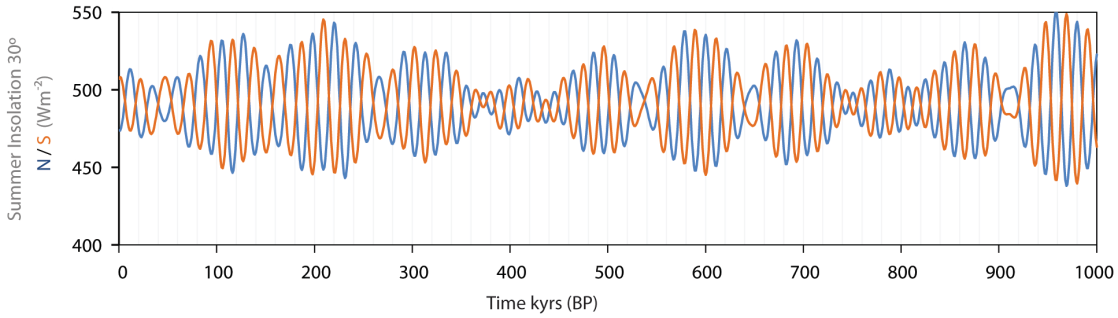

Fig. S1: *Summer insolation variations at 30°N (blue) and 30°S (red) over the last million years. Demonstrating the eccentricity modulation of precession at 100-kyr and 400-kyr periodicities. Data from Berger and Loutre (1991).*

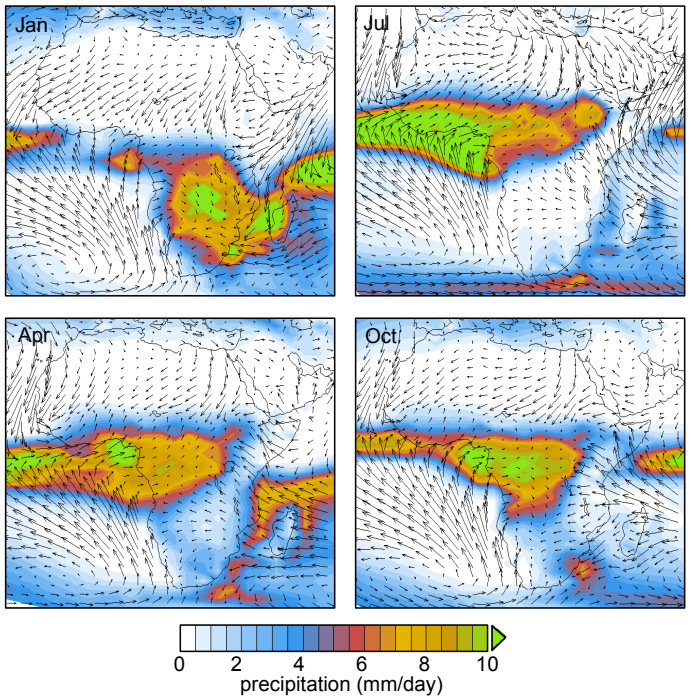

Fig. S2: Seasonal monthly mean precipitation and 10m winds for the HadCM3 pre-industrial simulation.

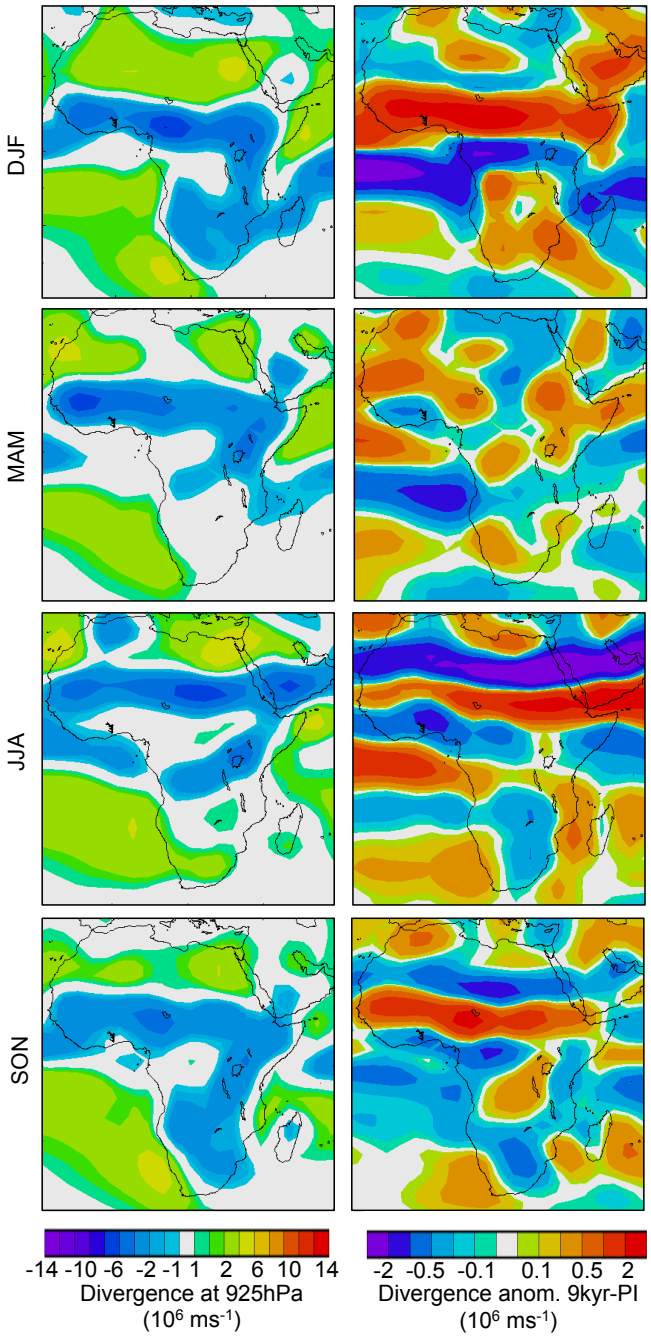

Fig. S3: (left) *Seasonal mean divergence at 925hPa from the Pre-industrial (PI) HadCM3 simulation for DJF, MAM, JJA, and SON seasons from top to bottom;* ***(right)*** *9kyr-PI convergence anomalies at 925hPa.*

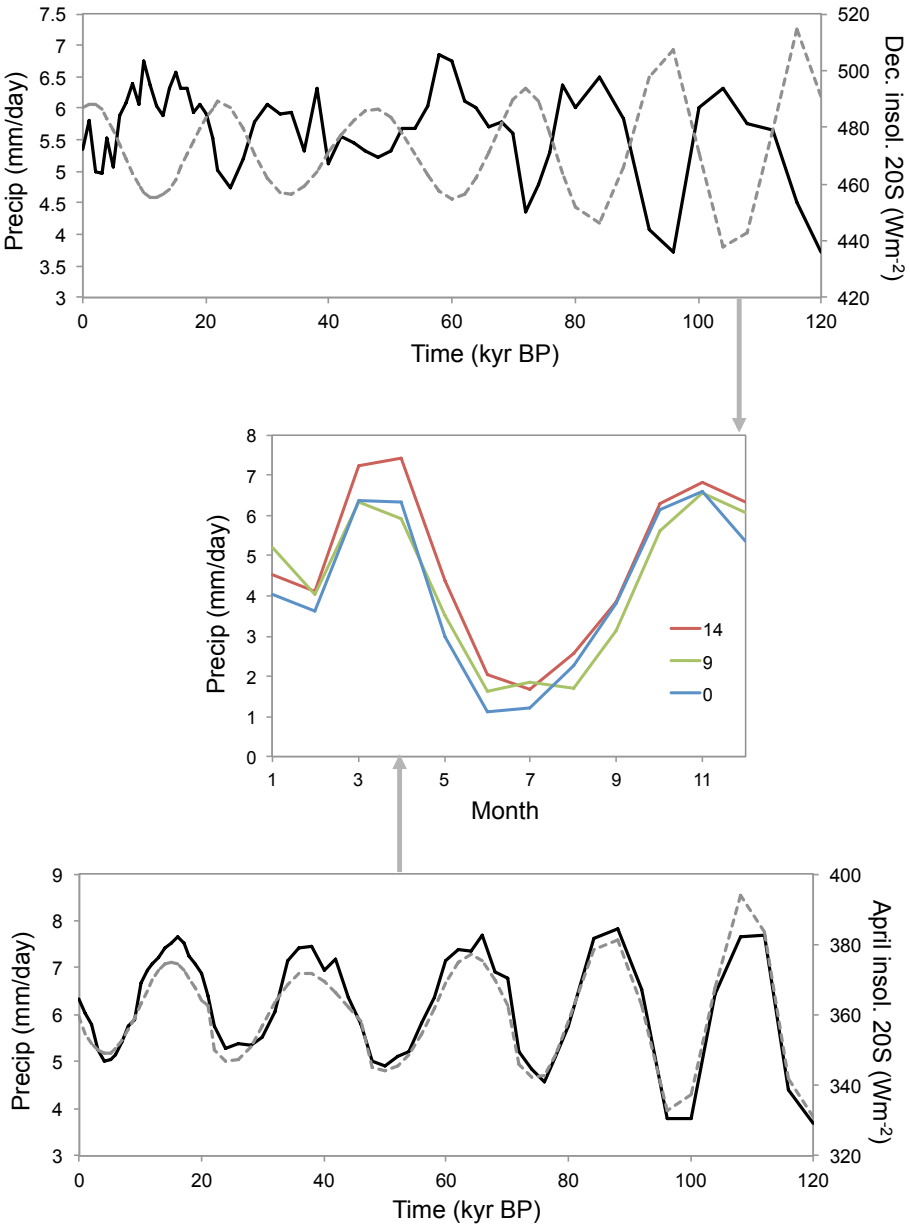

***Fig. S4**: Seasonality of West Africa precipitation from the ALL experiment. (Middle) Seasonal cycle of precipitation for 15-5°S 0-15°E, over land only, showing a double peak pattern. (Top) Precipitation from the same region for December through the last 120 kyr (solid line) is out of phase with local insolation for the same month (dotted line). (Bottom) Conversely, April precipitation (solid line) is in phase with local insolation for that month (dotted line).*

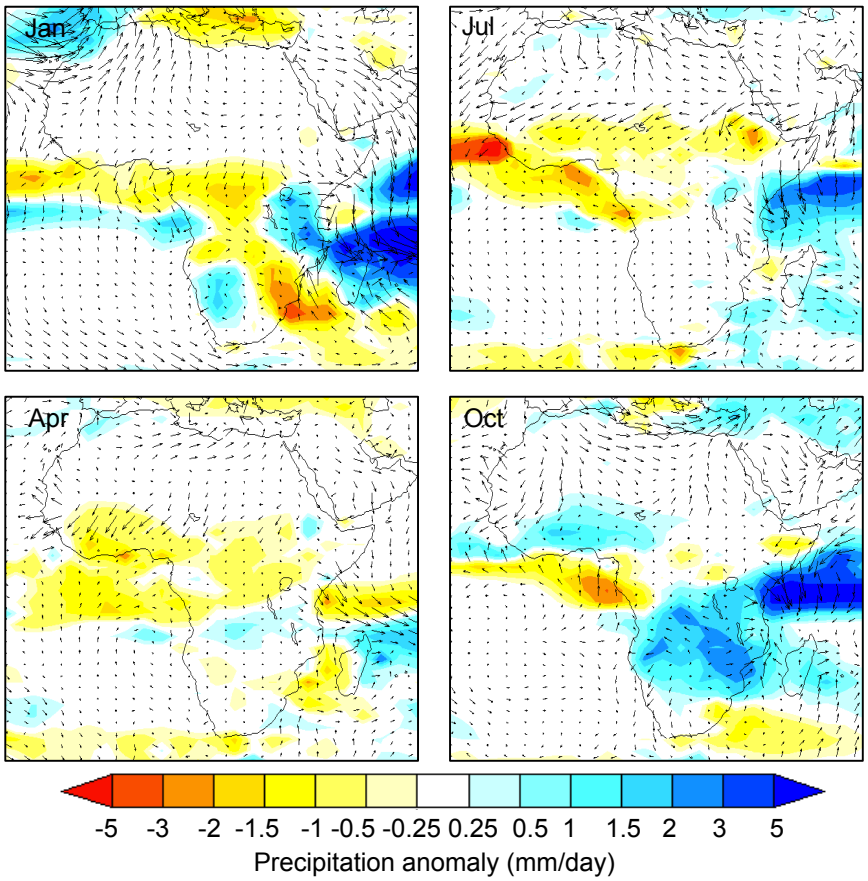

Fig. S5: *Seasonal mean precipitation and 10m wind anomalies for 21kyr-PI in the HadCM3 simulations represented by January, April, July, and October means (anticlockwise from top left). Fig. S8 shows the HadCM3 PI precipitation and winds for comparison.*

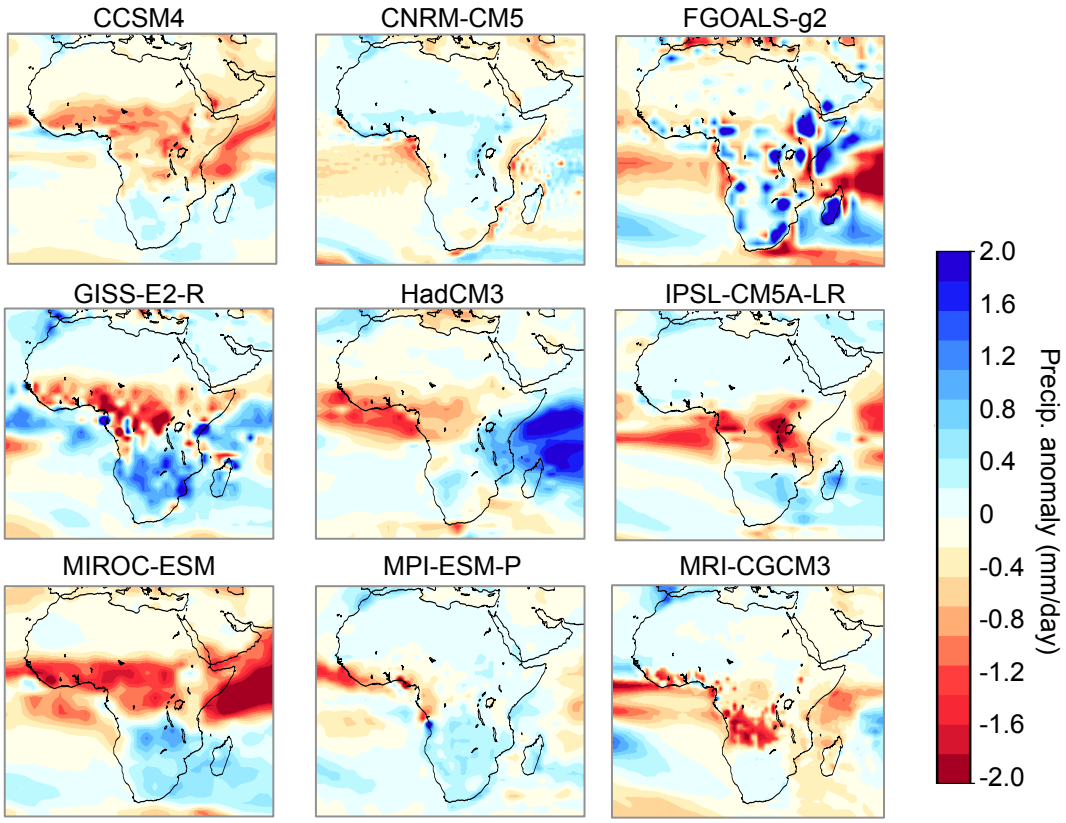

Fig. S6: *Mean Annual Precipitation anomalies for LGM-PI in mm/day for available PMIP3/CMIP5 models and HadCM3*

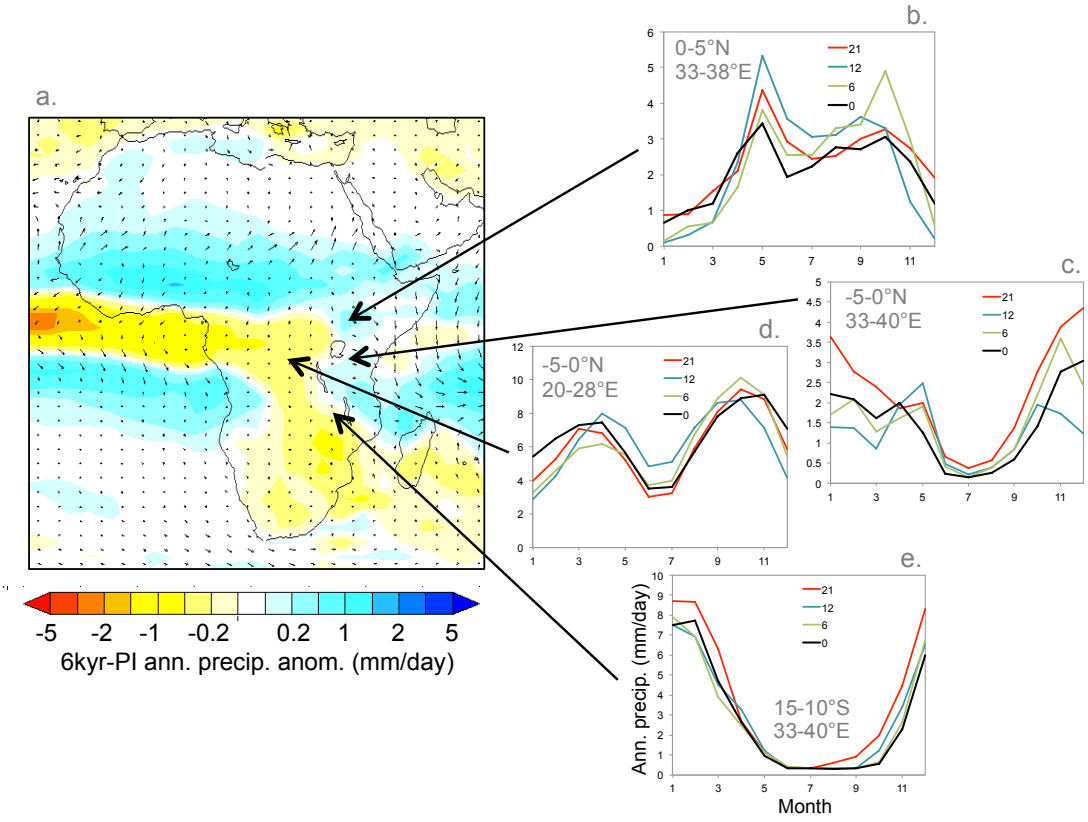

Fig. S7: *(a) annual mean precipitation and 10m wind anomalies for MH-PI; (b,c,d,e) seasonal cycle of precipitation over eastern and central African locations given in each sub-figure for PI (black), MH (6kyr, green), 12kyr BP (blue), and LGM (21kyr, red). Locations of area averaging are given in the sub-figures.*

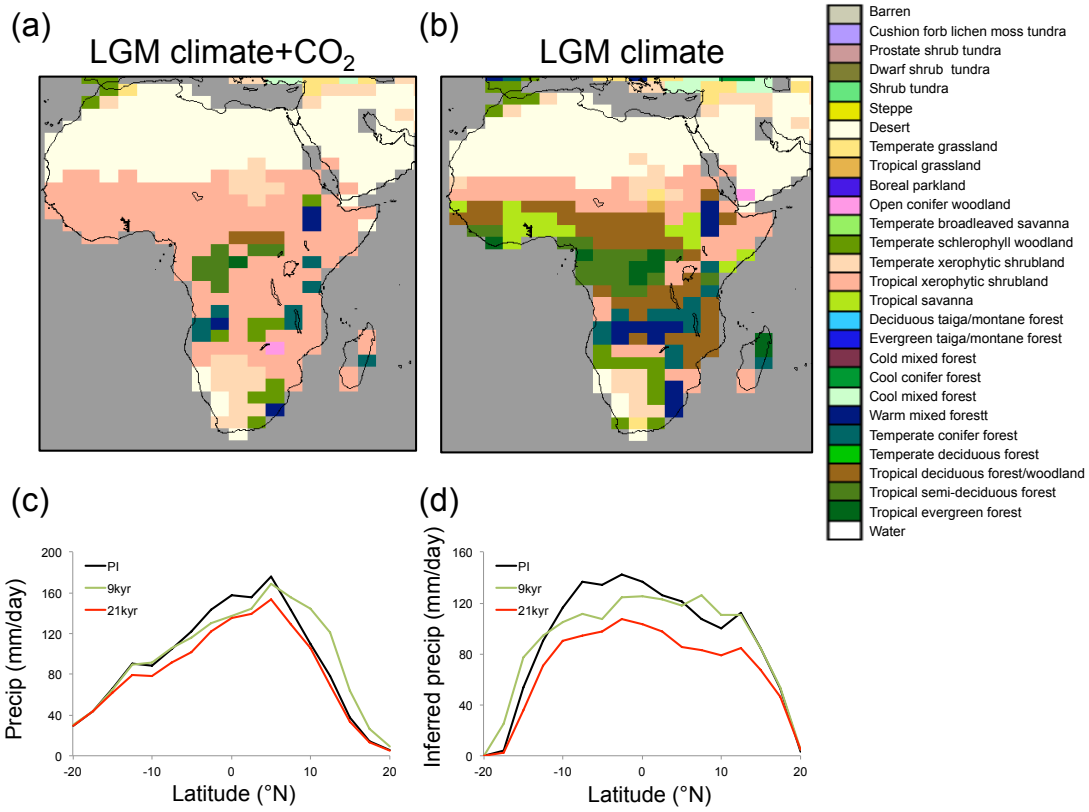

Fig. S8: *(a) biomes simulated with the Biome4 model (Kaplan et al., 2003) driven by climate LGM HadCM3 climate and LGM atmospheric CO_2 of 180ppm; (b) biomes simulated with Biome4 for the LGM driven by LGM HadCM3 climate and modern atmospheric CO_2 of 340ppm; (c) HadCM3 annual mean precipitation over land for latitudes between 20°S and 20°N averaged between 15°W and 20°E for PI (black), early Holocene (9kyr BP, green), and LGM (21kyr BP, red); (d) inferred precipitation for the same time slices and regions as (c) but using modern correlation between C3/C4 plant functional type net primary productivity (NPP) ratios and annual mean precipitation, and then using this correlation to infer precipitation at palaeo time slices from the Biome4 modelled C3/C4 NPP ratios. Plot (d) recreates the method for reconstructing rainfall used by Collins et al., 2011.*

Long	Lat	Core or Site ID	Proxy	21 ka	9 ka	4 ka	Reference
37.4	12.0	Lake Tana	δD_{wax}	na	1	-1	Costa et al (2014), QSR
37.4	12.0	Lake Tana	Magnetic, geochemical and seismic	na	1	-1	Marshall et al., (2011) Glob & Planetary Change
44.3	12.0	Gulf of Aden (P178-15P)	δD_{wax}	-1	1	0	Tierney and Demenocal (2013) Nature
41.6	11.1	Lake Abhe	Lake level	1	1	-1	Street-Perrott et al., (1989); COHMAP members, (1994) Oxf Lake levels database
37.0	4.7	Lake Chew Bahir	Geochemistry	-1	1	-1	Foerster et al (2012), Quat. Int.
36.1	3.6	Lake Turkana	Lake level	-1	1	1	Street-Perrott et al., 1989; COHMAP members, 1994 Oxf Lake levels database
33.0	-0.3	Lake Victoria	Diatom assemblage	na	1	1	Stager et al (2002), PPP, Stager et al., (1997), Quat. Res.
36.2	-0.4	Lake Nakuru-Elementaita	Lake level	-1	1	-1	Street-Perrott et al., (1989); COHMAP members, (1994) Oxf Lake levels database
36.3	-0.7	Lake Naivasha	Lake level	1	1	-1	Street-Perrott et al., (1989); COHMAP members, (1994) Oxf Lake levels database, Trauth et al., (2003), EPSL
33.2	-1.2	Lake Victoria	δD_{wax}	na	1	-1	Berke et al., (2012), QSR
37.7	-3.3	Lake Challa	δD_{wax}	1	1	-1	Tierney et al., (2011) QSR
37.7	-3.3	Lake Challa	BIT index	-1	1	1	Verschuren et al. (2009) Nature
29.5	-3.5	Eastern central Africa	Pollen	-1	0	0	Bonnefille. & Chalie (2000) Glob & Planetary Change
35.8	-3.9	Lake Manyara	Lake level	1	1	0	Street-Perrott et al., (1989); COHMAP members, (1994) Oxf Lake levels database
29.8	-6.7	Lake Tanganyika	δD_{wax}	-1	1	0	Tierney et al. (2008) Science
29.8	-6.7	Lake Tanganyika	Geochemistry	-1	1	1	Felton et al. (2007), PPP
32.8	-8.4	Lake Rukwa	Diatom assemblage	-1	1	0	Barker et al., (2002) PPP
30.8	-8.5	Lake Tanganyika	Diatom assemblage	-1	1	na	Gasse et al., (1989) Nature;
29.8	-9.1	Lake Cheshi	Lake level	0	1	0	Stager (1988) Quaternary Research
33.8	-9.3	Lake Masoko	Magnetic susceptibility, pollen	1	0	-1	Garcin et al., (2006) Geophys. Research Letters
33.8	-9.3	Lake Massoko	Diatom assemblage	-1	1	0	Barker et al., (2003), QR
34.2	-10.0	Lake Malawi	Diatom ^{18}O, palmatic acid δD	0	1	-1	Barker et al. (2007), EPSL
34.2	-10.0	Lake Malawi	Diatom assemblage	-1	0	0	Gasse et al., 2002 in Barker, P. A. &

							Gasse, F. (2003) QSR
34.3	-10.3	Lake Malawi	d13Cwax	-1	-1	1	Castañeda, et al., (2007), Geology
34.4	-11.3	Lake Malawi	δD_{wax}	1	-1	-1	Konecky et al. (2011) Earth and Planetary Science Letters
35.5	-15.5	Lake Chilwa	Lake level	1	1	na	Thomas et al., (2009) QSR
37.9	-18.2	Zambezi basin (offshore delta)	δD_{wax}	1	-1	0	Wang, Y. et al. (2012) Geochimica et Cosmochimica Acta
37.4	-18.6	Zambezi basin (offshore delta)	δD_{wax}	na	-1	-1	Schefuß, et al. (2011)

Table S1: Site data used in figure 10. Categories represent 1 (drier), 0 (no change) or -1 (drier) in relation to a late Holocene (0-2ka) mean for the timeslices 21 ka, 9 ka and 4 ka. Where the raw data timeseries was unavailable we used the interpretation in the text of the original publication. 'na' indicates the data were not available or do not extend to cover the timeslice of interest.

References

Barker, P., and Gasse, F. (2003). New evidence for a reduced water balance in East Africa during the Last Glacial Maximum: Implication for model-data comparison. Quaternary Science Reviews 22, 823-837.

Barker, P., Telford, R., Gasse, F., and Thevenon, F. (2002). Late pleistocene and holocene palaeohydrology of Lake Rukwa, Tanzania, inferred from diatom analysis. Palaeogeography, Palaeoclimatology, Palaeoecology 187, 295-305.

Barker, P., Williamson, D., Gasse, F., and Gibert, E. (2003). Climatic and volcanic forcing revealed in a 50,000-year diatom record from Lake Massoko, Tanzania. Quaternary Research 60, 368-376.

Barker, P. A., Leng, M. J., Gasse, F., and Huang, Y. (2007). Century-to-millennial scale climatic variability in Lake Malawi revealed by isotope records. Earth and Planetary Science Letters 261, 93-103.

Berke, M. A., Johnson, T. C., Werne, J. P., Grice, K., Schouten, S., and Sinninghe Damsté, J. S. (2012). Molecular records of climate variability and vegetation response since the Late Pleistocene in the Lake Victoria basin, East Africa. Quaternary Science Reviews 55, 59-74.

Bonnefille, R., and Chalie, F. (2000). Pollen-inferred precipitation time-series from equatorial mountains, Africa, the last 40 kyr BP. Global and Planetary Change 26, 25-50.

Castañeda, I. S., Werne, J. P., and Johnson, T. C. (2007). Wet and arid phases in the southeat African tropics since the Last Glacial Maximum. Geology 35, 823-826.

COHMAP Members, 1994, Oxford Lake Levels Database. IGBP PAGES/World Data Center-A for Paleoclimatology Data Contribution Series # 94-028. NOAA/NGDC Paleoclimatology Program, Boulder CO, USA.

Costa, K., Russell, J., Konecky, B., and Lamb, H. (2014). Isotopic reconstruction of the African Humid Period and Congo Air Boundary migration at Lake Tana, Ethiopia. Quaternary Science Reviews 83, 58-67.

Felton, A. A., Russell, J. M., Cohen, A. S., Baker, M. E., Chesley, J. T., Lezzar, K. E., McGlue, M. M., Pigati, J. S., Quade, J., Curt Stager, J., and Tiercelin, J. J. (2007). Paleolimnological evidence for the onset and termination of glacial aridity from Lake Tanganyika, Tropical East Africa. Palaeogeography, Palaeoclimatology, Palaeoecology 252, 405-423.

Foerster, V., Junginger, A., Langkamp, O., Gebru, T., Asrat, A., Umer, M., Lamb, H. F., Wennrich, V., Rethemeyer, J., Nowaczyk, N., Trauth, M. H., and Schaebitz, F. (2012). Climatic change recorded in the sediments of the Chew Bahir basin, southern Ethiopia, during the last 45,000 years. Quaternary International 274, 25-37.

Garcin, Y., Vincens, A., Williamson, D., Guiot, J., and Buchet, G. (2006). Wet phases in tropical southern Africa during the last glacial period. Geophysical Research Letters 33.

Gasse, F., Barker, P., and Johnson, T. C. (2002). A 24,000 yr diatom record from the northern basin of Lake Malawi. In "The East African Great Lakes: Limnology, Palaeolimnology and Biodiversity." pp. 393-414.

Gasse, F., Ledee, V., Massault, M., and Fontes, J.-C. (1989). Water-level fluctuations of Lake Tanganyika in phase with oceanic changes during the last glaciation and deglaciation. Nature 342, 57-59.

Konecky, B. L., Russell, J. M., Johnson, T. C., Brown, E. T., Berke, M. A., Werne, J. P., and Huang, Y. (2011). Atmospheric circulation patterns during late Pleistocene climate changes at Lake Malawi, Africa. Earth & Planetary Science Letters 312, 318–326.

Marshall, M. H., Lamb, H. F., Huws, D., Davies, S. J., Bates, R., Bloemendal, J., Boyle, J., Leng, M. J., Umer, M., and Bryant, C. (2011). Late Pleistocene and Holocene drought events at Lake Tana, the source of the Blue Nile. Global and Planetary Change 78, 147-161.

Schefuß, E., Kuhlmann, H., Mollenhauer, G., Prange, M., and Pätzold, J. (2011). Forcing of wet phases in southeast Africa over the past 17,000 years. Nature 480, 509-512.

Stager, J. C. (1988). Environmental changes at Lake Cheshi, Zambia since 40,000years BP. Quarternary Research 29, 54-65.

Stager, J. C., Cumming, B., and Meeker, L. (1997). A high-resolution 11,400-year diatom record from Lake Victoria East Africa. Quat. Res. 47, 81-89.

Street-Perrott, F.A., D.S. Marchand, N. Roberts, and S.P Harisson, 1989. Global Lake-Level Variations from 18,000 to 0 Years Ago: A Paleoclimatic Analysis. U.S. Department of Energy

Technical Report 46, Washington, D.C. 20545. Distributed by National Technical Information Service, Springfield, VA 22161.

Thomas, D. S. G., Bailey, R., Shaw, P. A., Durcan, J. A., and Singarayer, J. S. (2009). Late Quaternary highstands at Lake Chilwa, Malawi: Frequency, timing and possible forcing mechanisms in the last 44 ka. Quaternary Science Reviews 28, 526-539.

Tierney, J. E., and DeMenocal, P. B. (2013). Abrupt shifts in Horn of Africa hydroclimate since the last glacial maximum. Science 342, 843-846.

Tierney, J. E., Russell, J. M., Huang, Y., Sinninghe Damsté, J. S., Hopmans, E. C., and Cohen, A. S. (2008). Northern hemisphere controls on tropical southeast African climate during the past 60,000 years. Science 322, 252-255.

Tierney, J. E., Russell, J. M., Sinninghe Damsté, J. S., Huang, Y., and Verschuren, D. (2011). Late Quaternary behavior of the East African monsoon and the importance of the Congo Air Boundary. Quaternary Science Reviews 30, 798-807.

Trauth MH, Deino AL, Bergner AGN, et al. (2003) East Africam climate change and orbital forcing during the last 175 kyr BP. Earth and Planetary Science Letters 206: 297-313.

Verschuren, D., Sinninghe Damsté, J. S., Moernaut, J., Kristen, I., Blaauw, M., Fagot, M., and Haug, G. H. (2009). Half-precessional dynamics of monsoon rainfall near the East African Equator. Nature 462, 637-641.

Wang, Y. V., Larsen, T., Leduc, G., Andersen, N., Blanz, T., and Schneider, R. R. (2013). What does leaf wax δD from a mixed C3/C4 vegetation region tell us? Geochimica et Cosmochimica Acta 111, 128-139.